VNIR Multispectral Observations of Aqueous Alteration Materials by the Pancams on the Spirit and Opportunity Mars Exploration Rovers

William H. Farrand[1], Jeffrey R. Johnson[2], Melissa S. Rice[3], Alian Wang[4], James F. Bell III[5]

1. Space Science Institute, 4750 Walnut St., #205, Boulder, CO 80301
2. Johns Hopkins University Applied Physics Laboratory, 11100 Johns Hopkins Rd., Laurel, MD, 20723
3. Department of Geology, Western Washington University, 516 High St., Bellingham, WA, 98225
4. Department of Earth and Planetary Sciences, Washington University, Campus Box 1169, One Brookings Dr., St. Louis, MO, 63130
5. School of Earth and Space Exploration, Arizona State University, P.O. Box 87104Tempe, AZ, 85287

Submitted to American Mineralogist

Special section on Mars mineralogy

Submitted: November 17, 2015

Revision 1 submitted: February 3, 2016

Abstract

Multispectral visible and near infrared (VNIR) observations from the Mars Exploration Rover Pancam multispectral stereo camera systems are consistent with materials having been subjected to a variety of aqueous processes. Ferric oxides in the form of hematite in the Burns and Grasberg formations of Meridiani Planum have been well characterized by Opportunity on the basis of strong 535 and 864 nm absorptions and positive 754 to 1009 nm and 934 to 1009 nm slopes. On the Noachian-aged rim of Endeavour crater, Opportunity has observed light-toned veins with high Ca and S, as determined by the rover's Alpha Particle X-ray Spectrometer (APXS), and a negative 934 to 1009 nm slope in VNIR spectra extracted from Pancam, indicative of a 1000 nm H_2O overtone absorption- together these observations indicate that the veins are composed of gypsum. Rocks overturned by Opportunity on the Murray Ridge portion of the Endeavour crater rim display dark and light-toned coatings. The dark toned coatings have a red, featureless slope that is consistent with that observed in laboratory spectra of high valence manganese oxide minerals. Potential Mn oxide coatings may also be associated with some exposures of the Grasberg formation. APXS results for high Mg and S in the light-toned coatings of the Murray Ridge overturned rocks, and a negative 934 to 1009 nm slope are consistent with hydrated Mg-sulfates. Opportunity has also observed spectral features in rocks consistent with orbital observations of Fe-smectites, as well as Al-smectites and possible hydrated silica in light-toned fracture-fill materials. The Spirit rover observed sulfate-rich light-toned soils exposed by the rover's wheels. Several of these soil observations contained spectral features, such as a broad absorption centered near 800 nm, consistent with ferric sulfate minerals, a finding confirmed by the rover's Mössbauer spectrometer. Spirit also excavated light-toned Si-rich soils. These soils have a flat near infrared spectrum with a drop in reflectance from 934 to 1009 nm that is consistent with free water contained in voids or adsorbed onto the surface of the silica.

Keywords: Mars remote sensing, visible/near-infrared, Mars spectroscopy, iron oxides, ferric sulfates, manganese oxides, phyllosilicates

Introduction

Since January 2004, the Panoramic Cameras (Pancams) on-board the Mars Exploration Rovers Spirit and Opportunity have been imaging the martian surface along their traverse paths. A key objective of the Mars Exploration Rover (MER) mission has been to detect signs of ancient aqueous activity and determine the role of water in affecting geology at the two MER landing sites. The role of the Pancams has been to provide stereoscopic imaging to aid in the navigation of the rovers and to assess rock and outcrop morphology. The Pancams also possess multispectral imaging capability through the use of their two 8-position filter wheels with filter band centers and widths listed in **Table 1**. Aside from neutral density filters and an empty position, there are 13 filters devoted to geology observations between the two "eyes" of the Pancam with 11 distinct (non-overlapping) wavelengths from 432 to 1009 nm. From a Pancam 13 filter ("13f") observation, we obtain an image cube that provides a visible-to-near-infrared (VNIR) spectrum for each picture element, or pixel, for a total of 1024x1024 pixels in the imaged scene. This multispectral imaging enables us to characterize the VNIR reflectance character of targets of interest. The remote sensing aspect of Pancam has also proven important in cases where a target cannot be reached by the rover's robotic arm for *in situ* examination or where other operating constraints might preclude such an *in situ* examination.

This paper describes the Pancam instrument, data calibration, and how reflectance spectra from multispectral Pancam observations have been used to help constrain the identity of a number of minerals produced through aqueous alteration. The observations and results portion of the paper is divided according to several mineral and material groups: oxides, hydrous sulfates, hydrated silica, and presumed phyllosilicate-bearing rocks.

Examining how the VNIR multispectral imaging capabilities on the Spirit and Opportunity rovers have been used to characterize minerals associated with aqueous alteration is relevant for ongoing studies by the MSL rover Curiosity (Bell et al., 2013; Wellington et al., this issue), as well as similar capabilities planned for the ExoMars (e.g., Cousins et al., 2012) and Mars 2020 rovers. This paper also examines a number of spectrally distinctive materials observed by Opportunity since its departure from the Cape York rim segment of Endeavour crater. This paper furthers the multispectral examination of surface materials at Endeavour crater that was introduced in Farrand et al. (2013a, 2014) and is discussed in part by Arvidson et al. (this issue).

The Pancam Instrument and Calibration of Data

The Pancam instrument was described in detail by Bell et al. (2003). A description of mission operational calibration was provided by Bell et al. (2006). In brief, the Pancam on each rover has two 1024 by 1024 active-area charge-coupled devices (CCDs) with a 30 cm stereo separation and a 0.27 mrad per pixel resolution. Each Pancam is mounted 1.5 m above the ground on the mast referred to as the Pancam Mast Assembly (PMA). Each rover is also equipped with identical calibration targets (Bell et al., 2003) for the Pancam observations. Each Pancam was calibrated before launch (Bell et al., 2003; 2006). Operational surface procedures for the collection of multispectral images involve the close-in-time imaging of the calibration target (in extended mission operations with Opportunity, calibration target imaging is sometimes omitted if the calibration target was imaged on the previous sol at a similar time; acceptable given the relatively uniform atmospheric conditions from sol-to-sol on Mars). Multispectral image data from the calibration target, in conjunction with pre-launch calibration information, are utilized to convert raw image data to calibrated radiance and then to radiance factor (I/F, or more properly $I/\pi F$, where I is the measured radiance and πF is the incident solar irradiance).

Accumulation of airfall dust on the calibration target over the course of the mission led to development of a correction for dust on the calibration target based on a two-layer Hapke model along with the known photometric properties of the calibration target (Bell et al., 2006, Sohl-Dickstein et al., 2005). The measurements presented here are I/F divided by the cosine of the incidence angle at the time of image acquisition, a quantity described as relative reflectance, or R*, by Reid et al. (1999) and Bell et al. (2006). Bell et al. (2006) estimated that the absolute reflectance levels of Pancam multispectral data are accurate to within ~10% at the shortest wavelengths, and slightly more accurate at longer wavelengths. Relative filter-to-filter uncertainties in R* were estimated to be smaller, typically 1-5%, providing confidence in the reality of even very small-scale spectral variations detected in the scene. The 13-geology filter data sets examined here were typically compressed using the ICER wavelet-based compression routine (Kiely and Klimesh, 2003) so that blue stereo bands (the L7 and R1 bands) were at 2 bits-per-pixel and all other bands were at 1 bit-per-pixel for transmission and uncompressed back to the full dynamic range once received on Earth. Effects on the radiometric precision due to the compression were estimated to be < 1% based on pre-launch tests (Bell et al., 2006).

Multispectral Processing Tools Used on Pancam Spectra

Multispectral Approaches

Analysis of Pancam data has been performed using both image processing and spectral analysis paradigms. The image processing approach consists of successive analyses of the separate multispectral sequences of the left and right eye image data. Purely spectral analysis has been conducted using combined eye spectra of materials of interest that have been compiled and examined as 11 band datasets. As described in Farrand et al. (2006, 2007, 2008, 2013a, 2014), the use of a number of established image processing approaches has been applied to left- and/or right-eye image sequences including decorrelation stretch composites, spectral parameterization, spectral mixture analysis (Farrand et al., 2006), and supervised classification approaches. These techniques have been used to define regions of interest (ROIs) over spectrally distinctive or representative areas. Spectra from the ROIs in both the left and right eye data are averaged and are combined at the L2 and R2 bands (at 753 to 754 nm). These combined-eye spectra have been used for 11-band processing of assemblages of spectra. The combined-eye spectra have been analyzed as collections of vectors using clustering approaches (Anderson and Bell, 2013; Farrand et al., 2013a; 2014) and various endmember determination approaches (Farrand et al., 2008; 2013a; 2014).

Spectral Parameters

Spectral parameters are used to summarize information related to specific spectral characteristics such as slope, band depth, and the position of spectral features. **Table 2** lists a number of spectral parameters that have been used in various Pancam data analyses (e.g., Farrand et al., 2006, 2007, 2008, 2013, 2014; Rice et al., 2010).

Geologic Setting

The aqueous alteration minerals observed by Spirit and Opportunity are best understood in the geologic context of the Gusev crater and Meridiani Planum sites examined by these rovers. Overviews of the geology of Gusev crater as it was known prior to the landing of Spirit include Cabrol et al. (2003) and Greeley et al. (2003). In this paper, we focus on materials observed by Spirit on the Husband Hill peak of the Columbia Hills and in the Inner Basin and Home Plate which lie to the south of Husband Hill (images of Spirit’s traverse and site locations are available in Arvidson et al. (2008)). The materials in the Columbia Hills have been interpreted as being Noachian in age (Squyres et al., 2006). The materials making up Home Plate, at least its lower Barnhill unit, were interpreted by Squyres et al. (2007) as being pyroclastic, potentially hydrovolcanic, in origin. Sulfate-rich and silica-rich soils and nodules observed around Home Plate have been interpreted as being the result of hydrothermal processes (Schmidt et al., 2009; Ruff et al., 2011).

The geology of Terra Meridiani, and the Meridiani Planum subregion examined by Opportunity, were discussed prior to Opportunity's landing by Arvidson et al. (2003). From the time of its landing to its arrival at the rim of Endeavour crater, Opportunity explored the Burns formation, named in honor of geochemist Roger Burns, which comprise the bedrock of Meridiani Planum. The Burns formation is a sulfate-bearing "sandstone" composed of siliciclastic materials derived from the mechanical and chemical erosion of basalt (Grotzinger et al., 2005; McLennan et al., 2005; Clark et al., 2005). The Burns formation has been interpreted as being late Noachian to early Hesperian in age (Arvidson et al., 2006). The rim of the 22 km diameter Endeavour crater, which is currently the subject of Opportunity's explorations, has been interpreted as being Noachian in age (Squyres et al., 2012). Orbital observations made with the Mars Reconnaissance Orbiter (MRO) Compact Reconnaissance Imaging Spectrometer for Mars (CRISM) instrument revealed the presence of Fe/Mg smectite minerals on the rim of Endeavour (Wray et al., 2009; Noe Dobrea et al., 2012). Discussion of place names and units as well as traverse maps are provided in Squyres et al. (2012), Arvidson et al. (2014), and Crumpler et al. (2015). Observations by Opportunity around the bench of the raised rim segments revealed the presence of another sulfate-bearing stratigraphic unit that is chemically distinct from the Burns formation, the Grasberg formation (Crumpler et al., 2015). Other materials making up the rim of

Endeavour included an impact breccia, dubbed the Shoemaker formation and nominally older, clay-bearing, materials of the Matijevic formation (Squyres et al., 2012).

Pancam Observations of Aqueous Alteration Minerals

Oxides

Ferric Oxides. Hematite (Fe_2O_3) is a mineral that is widespread on Mars (Bell et al., 1996). The airborne and dune-forming bright drift deposits that blanket much of the planet's surface contain nanophase hematite (Singer et al., 1982). Crystalline (red) hematite and coarsely crystalline (gray) hematite are not as widespread (or at least not as apparent from telescopic and orbital observations) and, when observed, are indicate aqueous alteration. Opportunity was targeted to land in Meridiani Planum on the basis of orbital observations by the Mars Global Surveyor (MGS) Thermal Emission Spectrometer (TES) of coarsely crystalline gray hematite in the Meridiani Planum region (Christensen et al., 2000). Before Opportunity's landing, the type of surface materials hosting the gray hematite was unknown. After landing, it became apparent through observations by the rover's Miniature Thermal Emission Spectrometer (Mini-TES) and, later, *in situ* observations by the rover's Mössbauer spectrometer that the gray hematite was hosted both in spherules, interpreted as concretions, weathering out of the light-toned sulfate-bearing Burns formation outcrop (Klingelhöfer et al., 2004) and disseminated within the Burns formation itself (Glotch et al., 2006).

The first grind into Burns formation outcrop by Opportunity's Rock Abrasion Tool (RAT) produced red cuttings from the grind (**Fig. 1A**). The cuttings and the abraded rock surface displayed spectra with a strong 535 nm band, a near infrared (NIR) absorption band with a minimum in the Pancam R4 (864 nm) band and strongly positive 754 to 1009 nm and 934 to

1009 nm slopes. These spectral parameters match that of red hematite. However, the narrower reflectance maximum and deeper band depth of laboratory hematite compared to the Pancam spectrum of the RAT grind (**Fig. 1B**) indicates the influence of nanophase hematite and possibly other Fe-bearing phases on the spectral shape.

The spherules, colloquially referred to by the rover team as "blueberries", have reflectance spectra with a strongly positive 934 to 1009 nm slope, and a reflectance minimum appearing in some blueberry spectra in the Pancam R4 (864 nm) and in others in the R5 (904 nm) band. These spectral characteristics are consistent with coarsely crystalline (dark red) hematite (**Fig. 2**), but not of specular hematite which has a flat reflectance spectrum in the Pancam spectral range (**Fig. 3**). The presence of a 864 to 904 nm absorption band in the blueberry spectra suggests that the surfaces of the blueberries either have a patina of red to dark-red hematite, possibly produced by wind-driven dust abrasion, or that the grain size of the hematite in the blueberries is less than approximately 90 μm (Lane et al., 1999).

As noted in Farrand et al. (2007), Burns formation rock surfaces could be divided into those that are lighter-toned to buff-colored in composites such as L357 (673, 535, 432 nm) or L256 (753,535, 432 nm) (**Fig. 4**), which had a higher 482 to 535 nm slope (and was labeled in that paper as the HFS class for **H**igher **F**our hundred eighty-two to 535 nm **S**lope). The redder or more purple (again in composites such as L357 or L256; **Fig. 4**), cleaner (nominally wind-abraded) Burns formation outcrop surfaces also have red hematite-like spectra (**Fig. 5a**) although the near-infrared (NIR) band is not as well-defined and the 754 to 1009 nm slopes are diminished. Nevertheless, these surfaces referred to in Farrand et al. (2007) as the "LFS" (for **L**ower **F**our hundred eighty-two to 535 nm **S**lope) Burns formation surfaces have elevated 535 nm band depths and 904 nm band depths relative to other surface materials.

The Grasberg formation was first encountered on the bench of the Cape York rim segment of Endeavour crater, and was interpreted alternatively as immediately underlying or overlying the Burns formation (Crumpler et al., 2015). Natural, wind abraded surfaces of the Grasberg formation have an even closer resemblance to red hematite (**Fig. 5b**) with stronger 535 nm band depths, polynomial-fitted NIR band minimums at shorter wavelengths, and steeper 754 to 1009 nm slopes (**Fig. 6**) than are observed in the "purple" (LFS) Burns formation surfaces (Farrand et al., 2014).

Manganese Oxides. On the Murray Ridge portion of the Endeavour crater rim south of Solander Point, a turn-in-place maneuver by Opportunity resulted in the overturning of at least two rocks and the moving of others (Arvidson et al., this issue). The smaller and larger of the overturned rocks were named respectively Pinnacle Island and Stuart Island (**Fig. 7**). The newly exposed surfaces of both rocks have two different coatings on them. Both rocks displayed a dark-toned coating with a red, featureless spectral slope (**Fig. 8A**) and also a lighter-toned coating spectrally similar to the gypsum veins and the Lihir/Esperance fracture-fill discussed below. The nature of the light-toned coating is discussed in section 5.2.3 below in the discussion of sulfate minerals. As shown in **Fig. 8b**, the dark coating spectrum resembles that of terrestrial desert varnish. Desert varnish is generally composed of birnessite ($(Na,Ca)_{0.5}(Mn^{4+}, Mn^{3+})_2)O_4{\cdot}1.5H_2O$) mixed with clay minerals and hematite (Potter and Rossman, 1979). The comparison here to desert varnish is purely a comparison of spectral shape and is not intended as a process analogue. Fox et al., (2015) and Arvidson et al. (this issue) have provided a comparison of the dark coatings to pure and mixed Mn oxide mineral reflectance spectra and found that the spectra of the dark coatings are consistent with high-valence-state Mn oxide minerals. Indeed, the Mn-rich nature of the dark coatings was confirmed by APXS investigation (Arvidson et al., this issue).

Possible Mn-oxide minerals have also been observed by Pancam and APXS at several locations in association with the Grasberg formation. These include several small two-toned rocks on the north end of Cape York (occurring among rocks of the Grasberg formation) observed on sol 3038, a large patch of material, potentially a coating, on the target Monjon examined by APXS on sol 3419, and also on rocks observed along the eastern border of the rim on the bench imaged on sols 3739. These materials appear blue in left-eye composites such as L256, **Fig. 9A**, and purple in right-eye composites such as R731 (**Fig. 9B**) and the 535 nm band depth of these coatings is very weak with comparison to other surface materials (**Fig. 9C**). The spectra of these coatings (**Fig. 10**) have a positive, featureless red slope in the NIR and a broad, weak 535 nm band in the visible wavelengths. The Monjon "blue" spectrum, and the other occurrences noted from sols 3038 and 3419, occur amongst representative rocks of the Grasberg formation. Grasberg formation rocks have spectra more typical of the Monjon sol 3419 "purple" spectrum (**Fig. 10** and also as shown in **Fig. 5B**). Mn in the blue-gray portion of the Monjon target was twice that of the purple portion when measured by the APXS on sol 3419 (R. Gellert, pers. comm.).

As noted by Arvidson et al. (this issue) and Lanza et al. (2014) the presence of high-valence Mn oxides is significant since such minerals are formed in highly oxidizing, aqueous environments. Moreover, the presence of Mn-rich minerals is a potential indicator of a habitable environment on account of their association with water and highly oxidizing conditions.

Sulfates

Sulfate-rich Soils Observed by Spirit. The first recognition of sulfate-rich soils by the Spirit rover was during the investigation of the Big Hole (sol 113-115) and Boroughs trench (sol 135-142) targets on the Gusev crater volcanic plains between Bonneville crater and the Columbia Hills (Haskin et al., 2005). Although sulfates (with a maximum > 20 mass % of the examined soils) were implied by APXS and Mössbauer data analyses of trench regolith (Wang et al., 2006), no spectral features of sulfates were identified in Pancam spectra because, as indicated by the APXS data, the major sulfates were spectrally neutral Mg sulfates, rather than Fe sulfates that exhibit characteristic absorption features in the VNIR spectral range.

Five major exposures of sulfate-rich soils, containing Fe-sulfates, were excavated from depths of ~10 cm by Spirit (Arvidson et al. 2008, 2011; Wang et al., 2008; Rice et al. 2011). The namesake location for this class of soils (e.g., Ming et al., 2008) was the Paso Robles site on the crest of the Cumberland Ridge portion of Husband Hill (sol 399-432). Although examples of these soils were encountered after Paso Robles, another example was not examined *in situ* again until Spirit reached the Inner Basin (to the north of Husband Hill) at the Dead Sea/Arad region (sol 721-728, **Fig. 11a**). The failure of the rover's right front wheel led to the excavation of the Tyrone target on the eastern side of Home Plate (sol 784-798, sol 864-1062, sol 1098-1306), the Hamilton target on the north side of Home Plate (sol 1804 – 1852), and the Ulysses target on the west side of Home Plate (sol 1864-2186). **Fig. 11B** shows the typical Pancam spectra of "yellow" and "white" Fe^{3+}-sulfate-rich soils of the Arad site. These light-toned soils were found to have SO_3 concentrations measured by the APXS of up to 38 wt.% (Ming et al., 2006; 2008). Mössbauer spectrometer data indicated ferric-bearing sulfates in these soils (Morris et al., 2008), and the soils' distinctive Pancam and Mini-TES spectra are consistent with a heterogeneous mixture of hydrated ferric sulfate phases (*e.g.*, Johnson et al., 2007; Lane et al., 2008; Ruff et al., 2008; Arvidson et al., 2011).

Johnson et al. (2007) selected six typical Pancam spectra from the sulfate-bearing exposed soils at the Paso Robles, Dead Sea, and Tyrone sites, and used a database of 84 laboratory spectra and a multiple end-member spectral mixing model approach to identify candidate Fe-sulfate assemblages that may contribute to the observed Pancam spectra. Among the sulfate and ferric oxide/oxyhydroxide mineral spectra in the database, they found six ferric sulfates that could make significant contributions to the observed Pancam spectra. They are ferricopiapite [$Fe_{2/3}^{2+}Fe_4^{3+}(SO_4)_6(OH)_2{\cdot}20H_2O$], hydronium jarosite [$(H_3O)Fe_3^{3+}(SO_4)_2(OH)_6$], fibroferrite [$Fe^{3+}(SO_4)(OH){\cdot}5H_2O$], rhomboclase $HFe^{3+}(SO_4)_2{\cdot}4H_2O$], paracoquimbite [$Fe_2^{3+}(SO_4)_3{\cdot}9H_2O$], and a mixture of anhydrite [$CaSO_4$] with coquimbite [$Fe_2^{3+}(SO_4)_3{\cdot}9H_2O$]. The analyses of Johnson et al. (2007) suggested that ferricopiapite, hydronium jarosite, fibroferrite, rhomboclase composed a significant fraction of Tyrone yellowish light-toned soil, while fibroferrite, (anhydrite + coquimbite), and paracoquimbite were consistent with spectra of Paso Robles whitish light-toned soil, and hydronium jarosite and fibroferrite were likely present in Arad soils at the Dead Sea site (Johnson et al., 2007). **Fig. 12** compares a Pancam spectrum of Arad soil and library spectra of phases suggested by Johnson et al. (2007). Other minerals have been suggested as important components of the soils, including Fe^{3+}-bearing phosphates (Lane et al., 2008), hydrated silica (Wang et al., 2008), and elemental sulfur (Morris et al., 2008). These ferric sulfates are considered to be precipitates from a Fe^{3+} and SO_4-rich hydrothermal brine (Wang et al., 2008) or to have formed directly from fumarolic processes (Yen et al., 2008).

Wang et al. (2008) suggested that some of these minerals may be unstable under present Mars surface temperature and pressure conditions, and that repeated Pancam observations on exposed light-toned soils at Tyrone indicated spectral changes, namely a decrease in the spectral slope from the L7 (432 nm) to L3 (673 nm) bands, consistent with ferric sulfate phase changes. Specifically, laboratory experiments (Wang and Ling, 2011) on the stability and phase transformation of ferricopiapite (a potential component of Tyrone yellowish soils based on Johnson et al., 2007) demonstrated that under Mars-relevant conditions, the potential dehydration products of ferricopiapite are rhomboclase, kornelite $Fe_2^{3+}(SO_4)_3{\cdot}7H_2O$, pentahydrate $Fe_2^{3+}(SO_4)_3{\cdot}5H_2O$, paracoquimbite, and two types of amorphous ferric sulfates. Wang and Ling (2011) found reductions of the L3 vs. L7 ratio reflectance in laboratory sulfate dehydration studies similar to those noted by Wang et al. (2008) in the Tyrone yellow sulfate-bearing soils. The dehydration of ferricopiapite in Tyrone yellowish soil after exposure would suggest a very different temperature and relative humidity environment within the subsurface. In another examination of the data, Rice et al. (2011) studied the same Pancam observations and concluded that temporal variations in Pancam spectra were more consistent with deposition of airfall dust than with mineralogical changes, suggesting that the bright soils were stable over the observation timescales (100+ sols). Further analysis of these data appear warranted to resolve differences in interpretation.

Finally, the presence of a drop in reflectance from the 934 (R6) to 1009 nm (R7) band in some of the sulfate-bearing soils (such as the Arad white soil spectrum in **Fig. 11B** and **Fig. 12**) is potentially evidence of the presence of a water overtone feature centered near 1000 nm. This drop in reflectance was recognized as a feature of the Tyrone white soils by Wang et al. (2008) and was discussed as a possible hydration feature by Wang et al. (2008) and Wang and Ling (2011).

Ca-Sulfate Minerals Encountered by Opportunity. Most of Opportunity's traverse on the flat terrain of Meridiani Planum was over sulfate-bearing bedrock, as confirmed by Mössbauer (Klingelhöfer et al., 2004) and Mini-TES observations (Glotch et al., 2006). However, spectral features in the Pancam VNIR spectral range that could clearly be assigned to sulfate minerals in the Burns formation bedrock of Meridiani Planum were lacking. Upon reaching the rim of Endeavour crater, Opportunity has encountered at least two types of sulfate-bearing materials which have spectral features observable in the Pancam spectral range: gypsum veins and light-toned subsurface rock coatings.

In its traverse over the Cape York rim segment of Endeavour crater, examples of light-toned materials in linear to curvilinear veins were observed intermittently in Opportunity's Navcam images over the course of the traverse along Cape York. On the northwest bench of Cape York, Opportunity examined one of these veins *in situ*, the Homestake target (Squyres et al., 2012) (**Fig. 13**). Since that first examination, a number of veins have been examined *in situ* (most on the Endeavour rim bench unit). However, thinner veins on the Matijevic Hill portion of Cape York (in the Matijevic formation), and veins in the rim segments south of Cape York were also encountered. While displaying higher Ca and S in APXS results, the case for identifying the veins as consisting of the hydrated mineral gypsum [$CaSO_4$•2(H_2O)] was bolstered by the drop in reflectance from the Pancam R6 to R7 bands (934 to 1009 nm), which was attributed to a 1.0 μm H_2O overtone feature (Cloutis et al., 2006; Rice et al., 2010). The equivalent overtone feature in bassanite [CaSO4•0.5H_2O] occurs at 0.95 μm and anhydrite [$CaSO_4$] is anhydrous and thus does not have this absorption feature. Gypsum laboratory reflectance spectra convolved to the Pancam bandpasses show this 934 to 1009 nm drop in reflectance (**Fig. 14**). This drop in reflectance caused by a 1000 nm water overtone band has also been observed by multispectral imaging of light-toned veins using the Mastcam on the Mars Science Laboratory Curiosity rover (Vaniman et al., 2014; Wellington et al., this issue).

Ca-sulfates in the form of gypsum would precipitate at temperatures lower than basanite and anhydrite. The retaining of the highest hydration degree (as gypsum) is consistent with its extremely slow dehydration rate under current Mars surface conditions that was experimentally evaluated by Robertson and Bish (2013).

The gypsum veins observed by Opportunity are also characterized by high 535 nm band depth values. Terrestrial gypsum veins formed in ferric oxide-rich sediments often incorporate some of those ferric oxide-rich grains into the vein and this is likely the case with the veins observed on the Endeavour rim. Farrand et al. (2014) found spectral differences between the veins observed on the bench unit of Cape York and those occurring in the Matijevic Hill area. These two sets of veins also expressed differences when compared against the spectrally similar boxwork veins such as those hosting the Lihir and Esperance targets discussed below. The spectral differences between the bench unit veins, those on Matijevic Hill and the boxwork fracture fills are expressed primarily in terms of parameters related to the presence and/or degree of crystallinity of ferric oxide minerals such as 535 nm band depth and 754 to 1009 nm slope. **Fig. 15** shows a spectral parameter plot of the Cape York bench unit and Matijevic formation veins for the 754 to 1009 nm slope and 535 nm band depth parameters indicating spectral differences between the two sets of veins. The Matijevic formation veins have an overall flatter NIR spectral shape while the Cape York bench units have an overall red slope in the NIR leading to positive 754 to 1009 nm slopes. The higher 535 nm band depth of the Cape York bench veins also indicates a higher fraction of crystalline ferric oxides. Differences between the veins in terms of the parameter related to the 1000 nm hydration feature, the drop in reflectance from 934 to 1009 nm, are minimal as can be seen in Fig. 10 of Farrand et al. (2014). Spectral differences between the different sets of veins potentially indicate different episodes of fluid flow and vein formation.

Mg-Sulfates Encountered on Murray Ridge. Arvidson et al. (this issue) describe the Pinnacle Island and Stuart Island rocks overturned by Opportunity on the Murray Ridge portion of the Endeavour rim. As noted above, these rocks were characterized by both a dark, nominally Mn oxide-bearing coating and by a light-toned coating with a 934 to 1009 nm downturn in reflectance similar to that in the gypsum veins (**Fig. 16A**). As noted by Rice et al. (2010) a number of hydrated or hydroxylated minerals display a 1 μm overtone feature that at Pancam spectral resolution would display the R6 to R7 drop in reflectance.

The Pinnacle and Stuart Island APXS observations that were centered principally over the light-toned portions of those rocks showed high Mg and S values- indicating the presence of Mg sulfate minerals (Arvidson et al., this issue). Kieserite [$MgSO_4 \bullet H_2O$] and epsomite [$MgSO_4 \bullet 7H_2O$] both display drops in reflectance in the longest Pancam channel (**Fig. 16B**). For epsomite, the H_2O absorption is broader leading to a decrease in reflectance extending to Pancam's R6 (934 nm) and R5 (904 nm) bands. Hence, the multispectral evidence from Pancam is consistent with the light-toned coatings on Pinnacle and Stuart Island containing a Mg sulfate phase, potentially kieserite.

Hydrated Silica

One of the most striking discoveries of the Spirit mission was the discovery of nearly-pure hydrated silica in a subsurface soil in the "Eastern Valley" on the eastern side of Home Plate. The highest Si content (> 90 wt.%) was in the Gertrude Weise (**Fig. 17B**) soil target (Squyres et al., 2008). The "white" soils at the sulfate-bearing exposures Tyrone and Troy also were found to contain a SiO_2 component (Wang et al., 2008; Arvidson et al., 2011). SiO_2 made up 32.9% of the Mt. Darwin observation within the Tyrone soils (Ming et al., 2008) and up to 46% of the Tyrone soils (Arvidson et al., 2011). Friable, nodular outcrops containing significant amounts of hydrated silica (61.8 – 72.8 wt.%) were also observed in the vicinity of Home Plate (**Fig. 17A**). The Si-rich deposits have been alternatively interpreted as volcanic fumarolic deposits (Squyres et al., 2008) or as the result of precipitation from geothermal waters (Ruff et al., 2011; Wang et al., 2008). Recently morphologic similarities have been observed between the Si-rich nodules in the Eastern Valley and high-altitude silica sinter deposits in the El Tatio hot springs region in Chile (Ruff, 2015; Nicolau et al., 2014).

The soil and nearby silica-rich outcrops are spectrally distinct from other Gusev crater materials in VNIR wavelengths: Wang et al. (2008) identified a drop in reflectance from 934 to 1009 nm that characterizes Pancam spectra of all known hydrated silica targets observed by Spirit, which Rice et al. (2010) showed is due to the $2\nu_1 + \nu_3$ H_2O combination band and/or the 3ν OH overtone centered near ~1000 nm. In a study of these spectral features in terrestrial high-silica materials, Rice et al. (2013) showed that most opaline silica samples exhibit these features near ~950-960 nm, which is between Pancam's R6 and R7 filters and would thus be undetectable to the instrument. However, the spectra of water-saturated silica reproduce the spectral downturn at 1009 nm that characterizes the Pancam silica spectra, leading to the interpretation that the silica-rich materials observed by MER Spirit must contain large amounts of free water contained in voids or adsorbed onto the silica surface.

The silica-rich materials are characterized by flat NIR spectra from 864 to 934 nm, which allows the narrow hydration band to be distinguished from broad absorptions near 1000 nm in the spectra of iron-bearing minerals. The broader ferric or ferrous iron absorptions near 1000 nm result in lower reflectance in additional Pancam bands besides the R7 (1009 nm) band- e.g. these absorptions reduce the reflectance in the R6 (934 nm) down to the R4 (864 nm) bands, or to even shorter wavelengths. Using criteria based on these parameters, Rice et al. (2010) defined a Pancam "hydration signature" that characterizes the spectra of the hydrated minerals to which the instrument is sensitive (including hydrated silica, some hydrated Mg- and Ca-sulfates, water ice, and some carbonates). Rice et al. (2010) showed that the Pancam spectra of some dust-covered rock surfaces can mimic the hydration signature when tilted away from the rover's line of sight and/or when viewed at very low Sun elevations. To avoid these false detections, the Pancam hydration signature has typically only been used to identify potentially hydrated materials in observations made at low (~0°-30°) incidence (*i*) and emission (*e*) angles. The contributing factors to the negative 934 to 1009 nm spectral slope of these rock surfaces have not yet been fully identified, but Rice et al. (2010) proposed two main hypotheses: (1) the NIR slope is due to hydration in the Martian surface dust; or (2) the NIR slope effect is due to Pancam calibration inaccuracies at specific viewing geometries. Example hydrated silica outcrop and soils are shown in **Fig. 17C**. This Pancam hydration signature has since been used to interpret the mineralogy of other high-silica surface targets at Gusev crater (*e.g.*, Ruff et al., 2011; Arvidson et al., 2011) and hydrated Ca-sulfate at Meridiani Planum (Squyres et al., 2012; Farrand et al., 2013a, b, 2014) (Section 3.2.2.1).

Phyllosilicate-bearing Outcrops

By the time that Opportunity reached the rim of Endeavour crater, its instruments that were most sensitive to diagnostic mineral identification (Mössbauer spectrometer and Mini-TES), had ceased to function. However, through the orbital reflectance spectroscopy of CRISM and rover observations, the Whitewater Lake type outcrops of the Matijevic formation (**Fig. 18A** and **18B**) were identified as being the host of a weak Fe-smectite signature (Arvidson et al., 2014). Also, in its exploration of the Matijevic Hill area, Opportunity encountered morphologically distinctive boxwork structures (**Fig. 18C**). APXS examination of the light-toned fracture fill material of these structures indicated Al- and Si-rich compositions which geochemical modeling (Arvidson et al., 2014; Clark et al., this issue) was consistent with Al smectite compositions plus a potential hydrated silica component.

Pancam spectra of the Whitewater Lake type outcrops could be divided into the light-toned, fine-grained matrix materials exemplified by the Azilda IDD location (**Fig. 18A**) and the darker-toned coatings such as the Chelmsford IDD target (**Fig. 18B**). Spectra of these materials are shown in **Fig. 19.**

The light-toned matrix materials are characterized by a broad reflectance peak centered near 770 nm and negative slope from 864 to 1009 nm. The darker-toned coatings exhibit a more convex reflectance peak and weak near-infrared absorption centered near 950 nm and also a higher 535 nm band depth than the matrix materials. The deeper 535 and 904 nm band depths were noted by Farrand et al. (2014) as being consistent with the coatings having more partially to well-crystalline ferric iron minerals than are present in the matrix materials. Also, while not diagnostic of the presence of nontronite, a third degree polynomial fitted to the four bands from 864 to 1009 nm of the dark coatings has a median band minimum of 950 nm which is close to the continuum-removed band center of nontronite of 955 to 960 nm.

In an exploratory "walk-about" of Matijevic Hill, Opportunity observed the presence of boxwork structures in several locations. A prominent boxwork structure, with thick, light-toned fracture-fill materials was briefly examined with the rover's MI and APXS at the Lihir target. The APXS indicated that Lihir had the highest Al and Si yet detected in any target examined by

Opportunity to that time (Al_2O_3 of 12.92% and SiO_2 of 58.44%; Clark et al., this issue). Opportunity returned to this fracture fill in order to investigate it more fully with a RAT brush and grind on a new target, Esperance (yellow circle in **Fig. 18C**). The geochemistry of the Esperance target is described by Clark et al. (this issue). Pancam spectra of the Lihir/Esperance fracture fill resembled the gypsum veins observed on the bench of Cape York and on Matijevic Hill with a high reflectance, relatively high 535 nm band depth, and a convex shape in the NIR with a drop in reflectance from the Pancam R6 to R7 bands (934 to 1009 nm) (**Fig. 20**). However, in terms of more subtle spectral parameters, the boxwork fracture fills have lower 535 nm band depths and have a fifth degree polynomial fitted band position with a median position shorter than that of both sets of gypsum veins (**Fig. 21**).

Also, since geochemical modeling of Esperance has allowed for the possibility of excess silica (Clark et al., this issue), the presence of the 934 to 1009 nm drop of reflectance, suggests the presence of hydrated silica, potentially similar to that observed by Spirit in the Eastern Valley near Home Plate (section 3.3). Representative spectra from the Eastern Valley nodules (broken surfaces from the Innocent Bystander target which was rolled over by Spirit) are compared against a wind-abraded, light-toned portion of Esperance in **Fig. 22**. Although similar, the NIR reflectance of the Si nodules is flat whereas that of Esperance is more convex. Also, as shown in **Fig. 23**, the Si nodules have a lower 754 to 1009 nm slope and a higher R6/R7 (934/1009 nm) ratio compared to Esperance and Lihir measurements. If the 934 to 1009 nm drop in reflectance in Esperance is attributable to hydrated silica, the higher R6/R7 ratio of the Eastern Valley Si-rich nodules is nominally attributable to a higher fraction of hydrated silica (62 to 69% SiO_2 in the Innocent Bystander target) in the nodules compared to Esperance. Esperance has ~66% SiO_2, most of which Clark et al. (this issue) attribute to montmorillonite (which does not have the

934 to 1009 nm drop in reflectance when convolved to Pancam bandpasses), but the geochemical modeling of those authors attributes one-sixth to one-fourth of the SiO_2 to silica and thus Esperance would have a lower fraction of hydrated silica compared to the Eastern Valley silica nodules and this would be consistent with the lower R6/R7 ratio compared to the silica nodules.

Key Observations for Mineralogical Identifications

The multispectral reflectance measurements provided by the Pancam on both Spirit and Opportunity have provided complementary information on rocks and soils to that provided by the other MER instruments. Since the loss of Opportunity's Mini-TES and Mössbauer spectrometers, Pancam has become the only instrument on the rover providing mineralogical constraints. In this paper, we highlight instances in which Pancam multispectral observations have contributed to mineralogical identifications. These include:

1. The observation of red hematite in multiple locations visited by Opportunity including Burns and Grasberg formation outcrops and the gray hematite spherules, interpreted as concretions, that weather out of the Burns formation outcrop and that blanket the Meridiani Planum plains.

2. Dark coatings with a "red" (reflectance increasing with increasing wavelength) generally featureless slope that are consistent with Mn oxides. These coatings include more Mn-rich coatings on the overturned rocks Pinnacle and Stuart Island and the previously unreported on "blue" coatings on some Grasberg formation outcrops.

3. The observation of spectral features consistent with Fe-bearing sulfate minerals at several exposures of sulfur-rich soils excavated from the subsurface by the wheels of the Spirit rover and examined *in situ* by Spirit.

4. The 934 to 1009 nm drop in reflectance in Si-rich light toned soils and nodules in the Eastern Valley of the Home Plate region examined by Spirit have been attributed to free water contained in voids or adsorbed onto the surface of the silica associated with these materials.

5. The drop in reflectance associated with a 1 μm water overtone feature in gypsum veins on the bench of the Cape York rim segment of Endeavour crater, another set of gypsum veins exposed in the outcrop of Matijevic Hill, also on Cape York, and gypsum veins observed on the southern rim segment of Murray Ridge/Cape Tribulation.

6. The light-toned coatings on the overturned rocks Pinnacle and Stuart Island, which display enrichments in Mg and S as determined by the APXS, have a drop in reflectance from 934 to 1009 nm that is consistent with the spectra of some Mg sulfate minerals, specifically kieserite.

7. The 934 to 1009 nm drop in reflectance that is observed in gypsum veins was also observed in the Al and Si rich fracture fills in boxwork structures on Matijevic Hill. Based on APXS modeled geochemistry (Clark et al., this issue) this feature, also

attributed to a H_2O overtone absorption, is more likely caused by hydrated silica in the fracture fill material.

Implications

The ability to detect minerals altered by aqueous activity using visible and near-infrared (VNIR) multispectral imaging data on the surface of Mars has been demonstrated in this paper. This ability has relevance for the Opportunity's on-going exploration of the western rim of Endeavour Crater. The use of Pancam for the definition of spectrally unique materials is especially important in the near term for Opportunity's exploration of the Marathon Valley area where orbital data has indicated the presence of phyllosilicate minerals. Also, the potential to use VNIR multispectral imaging for the detection of aqueous alteration minerals also has importance for the use of the Curiosity rover's Mastcam and will be used in the future with the ExoMars PanCam and the Mars 2020 Mastcam-Z.

Acknowledgements

The first author is supported as a Participating Scientist on MER through the Jet Propulsion Laboratory. We would like to thank Ralf Gellert of the University of Guelph for helpful discussions on APXS results. We also thank Ed Cloutis and an anonymous reviewer for helpful reviews.

References

Anderson, R.B. and Bell, J.F. III (2013) Correlating multispectral imaging and compositional data from the Mars Exploration Rovers and implications for Mars Science Laboratory. Icarus, 223, 157-180.

Arvidson, R.E., Seelos, F.P. IV, Deal, K.S., Koeppen, W.C., Snider, N.O., Kieniewicz, J.M., Hynek, B.M., Mellon, M.T., and Garvin, J.B. (2003) Mantled and exhumed terrains in Terra Meridiani, Mars. Journal of Geophysical Research-Planets, 108, No. E12, doi: 10.1029/2002JE001982.

Arvidson, R.E., Ruff, S.W., Morris, R.V., Ming, D.W., Crumpler, L.S., Yen, A.S., Squyres, S.W., Sullivan, R.J., Bell, J.F. III, Cabrol, N.A., and others (2008) Spirit Mars Rover Mission to the Columbia Hills, Gusev Crater: Mission overview and selected results from the Cumberland Ridge to Home Plate. Journal of Geophysical Research-Planets, 113, E12S33, doi:10.1029/2008JE003183.

Arvidson, R.E., Ashley, J.W., Bell, J.F. III, Chojnacki, M., Cohen, J., Economou, T.E., Farrand, W.H., Fergason, R., Fleischer, I., Geissler, P., and others (2011) Opportunity Mars Rover mission: Overview and selected results from Purgatory ripple to traverses to Endeavour crater. Journal of Geophysical Research-Planets, 116, E00F15, doi:10.1029/2010JE003746.

Arvidson, R.E., Squyres, S.W., Bell, J.F. III, Catalano, J.G., Clark, B.C., Crumpler, L.S., De Souza, P.A., Fairen, A.G., Farrand, W.H., Fox, V.K., and Gellert, R. (2014) Ancient aqueous environments at Endeavour Crater, Mars. Science, 343, doi:10.1126/science.1248097.

Arvidson, R.E., Squyres, S.W., Morris, R.V., Knoll, A.H., Gellert, R., Clark, B.C., Catalano, J.G., Jolliff, B.L., McLennan, S.M., Herkenhoff, K.E., and others (2016) High concentration manganese and sulfur-bearing deposits on Murray Ridge, Endeavour crater, Mars. American Mineralogist, in press.

Bell, J.F III (1996) Iron, sulfate, carbonate, and hydrated minerals on Mars. In M.D. Dyer, C. McCammon, and M.W. Schaefer, Eds., Mineral Spectroscopy: A Tribute to Roger G. Burns, Geochem. Soc. Spec. Pub. No. 5, p. 359-380, Houston.

Bell, J.F. III, Squyres, S.W., Herkenhoff, K.E., Maki, J.N., Arneson, H.M., Brown, D., Collins, S.A., Dingizian, A., Elliot, S.T., Hagerott, E.C., and others (2003) The Mars Exploration Rover Athena Panoramic Camera (Pancam) Investigation. Journal of Geophysical Research-Planets, 108, doi:10.1029/2003JE002070.

Bell, J.F. III, Joseph, J., Sohl-Dickstein, J.N., Arneson, H.M., Johnson, M.J., Lemmon, M.T., and Savransky, D. (2006) In-flight calibration and performance of the Mars Exploration Rover Panoramic Camera (Pancam) instruments. Journal of Geophysical Research-Planets, 111, E02S03, doi:10.1029/2005JE002444.

Bell, J.F. III, Godber, A., Rice, M.S., Fraeman, A.A., Ehlmann, B.L., Goetz, W., Hardgrove, C.J., Harker, D.E., Johnson, J.R., Kinch, K.M., and others (2013) Initial multispectral imaging results from the Mars Science Laboratory Mastcam investigation at the Gale crater field site. 44th Lunar and Planetary Science Conference, abstract #1417.

Burns, R.G. (1987) Ferric sulfates on Mars. Proceedings of the 17th Lunar and Planetary Science Conference, Journal of Geophysical Research, 92, E570-E574.

Cabrol, N.A., Grin, E.O., Carr, M.H., Sutter, B., Moore, J.M., Farmer, J.D., Greeley, R., Kuzmin, R.O., DesMarais, D.J., Kramer, M.G., and others (2003) Exploring Gusev Crater with Spirit: Review of science objectives and testable hypotheses. Journal of Geophysical Research-Planets, 108 (E12), 8076, doi:10.1029/2002JE002026.

Christensen, P.R., Bandfield, J.L., Clark, R.N., Edgett, K.S., Hamilton, V.E., Hoefen, T., Kieffer, H.H., Kuzmin, R.O., Lane, M.D., Malin, M.C., and others (2000) Detection of crystalline hematite mineralization on Mars by the Thermal Emission Spectrometer: Evidence for near-surface water, Journal of Geophysical Research-Planets. 105, 9623-9642.

Clark, B.C., Morris, R.V., McLennan, S.M., Gellert. R., Jolliff, B.L., Knoll, A.H., Squyres, S.W., Lowenstein, T.K., Ming, D.W., Tosca, N.J. and Yen, A. (2005) Chemistry and mineralogy of outcrops at Meridiani Planum. Earth and Planetary Science Letters, 240, 73– 94.

Clark, B.C., Morris, R.V., Herkenhoff, K.E., Farrand, W.H., Gellert. R., Jolliff, B.L., Arvidson, R.E., Squyres, S.W., Mittlelfehldt, D.W., Ming, D.W., and Yen A. (2016) Esperance:

Multiple episodes of aqueous alteration involving fracture fills and coatings at Matijevic Hill, Mars. American Mineralogist, in press.

Clark, R.N., Swayze, G.A., Wise, R., Livo, E., Hoefen, T., Kokaly, R., and Sutley, S.J. (2007) USGS digital spectral library splib06a, U.S. Geological Survey, Digital Data Series 231.

Cloutis, E.A., Hawthorne, F.C., Mertzman, S.A., Krenn, K., Craig, M.A., Marcino, D., Methot, M., Strong, J., Mustard, J.F., Blaney, D.L., and Bell, J.F. (2006) Detection and discrimination of sulfate minerals using reflectance spectroscopy. Icarus, 184, 121-157.

Cousins, C.R., Gunn, M., Prosser, B.J., Barnes, D.P., Crawford, I.A., Griffiths, A.D., Davis, L.E. and Coates, A.J. (2012) Selecting the geology filter wavelengths for the ExoMars Panoramic Camera instrument. Planetary and Space Science, 71, 80-100, doi:10.1016/j.pss.2012.07.009.

Crumpler, L.S., Arvidson, R.E., Bell, J., Clark, B.C., Cohen, B.A., Farrand, W.H., Gellert, R., Golombek, M., Grant, J.A., Guinness, E., and Herkenhoff, K.E. (2015) Context of ancient aqueous environments on Mars from in situ geologic mapping at Endeavour Crater. Journal of Geophysical Research-Planets, 120, 538–569, doi:10.1002/2014JE004699.

Farrand, W.H., Bell, J.F. III, Johnson, J.R., Squyres, S.W., Soderblom, J., and Ming, D.W. (2006) Spectral variability among rocks in visible and near infrared multispectral Pancam data collected at Gusev Crater: Examinations using spectral mixture analysis and related techniques. Journal of Geophysical Research-Planets, 111, E02S15, 10.1029/2005JE002495.

Farrand, W.H., Bell, J.F. III, Johnson, J.R., Jolliff, B.L., Knoll, A.H., McLennan, S.M., Squyres, S.W., Calvin, W.M., Grotzinger, J.P., Morris, R.V. and Soderblom, J. (2007) Visible and near-infrared multispectral analysis of rocks at Meridiani Planum, Mars by the Mars Exploration Rover Opportunity. Journal of Geophysical Research-Planets, 112, E06S02, 10.1029/2006JE002773.

Farrand, W.H., Bell, J.F. III, Johnson, J.R., Arvidson, R.E., Crumpler, L.S., Hurowitz, J.A., and Schröder, C. (2008) Rock spectral classes observed by the Spirit rover’s Pancam on the Gusev crater plains and in the Columbia Hills, Journal of Geophysical Research-Planets. 113, E12S38, doi:10.1029/2008JE003237.

Farrand, W.H., Bell, J.F., Johnson, J.R., Rice, M.S., and Hurowitz, J.A. (2013a) VNIR multispectral observations of rocks at Cape York, Endeavour crater, Mars by the Opportunity rover’s Pancam. Icarus, 225, 709-725.

Farrand, W.H., Ruff, S.W., Rice, M.S., Rice, J.W. Jr., Arvidson, R.E., Jolliff, B.L., Squyres, S.W., Knoll, A.H., Bell, J.F. III, and Johnson, J.R. (2013b) Veins in Matijevic Hill lithologic units observed by Opportunity, 44th Lunar and Planetary Science Conference, abstract #2482.

Farrand, W.H., Bell, J.F. III, Johnson, J.R., Rice, M.S., Jolliff, B.L., and Arvidson, R.E. (2014) Observations of rock spectral classes by the Opportunity rover's Pancam on northern Cape

York and on Matijevic Hill, Endeavour Crater, Mars. Journal of Geophysical Research-Planets, 119, doi:10.1002/2014JE004641.

Fox, V.K., Arvidson, R.E., Jolliff, B.L., Carpenter, P.K., Catalano, J.G., Hinkle, M.A.G., and Morris, R.V. (2015) Characterization of synthetic and natural manganese oxides as martian analogues. 46th Lunar and Planetary Science Conference, abstract #2132.

Glotch, T.D., Bandfield, J.L., Christensen, P.R., Calvin, W.M., McLennan, S.M., Clark, B.C., Rogers, A.D., and Squyres, S.W. (2006) Mineralogy of the light-toned outcrop at Meridiani Planum as seen by the Miniature Thermal Emission Spectrometer and implications for its formation. Journal of Geophysical Research-Planets, 111, E12S03, doi:10.1029/2005JE002672.

Greeley, R., Kuzmin, R.O., Rafkin, S.C., Michaels, T.I., and Haberle, R. (2003) Wind-related features in Gusev crater. Mars, Journal of Geophysical Research-Planets, 108, 8087, doi:10.1029/2002JE002006.

Grotzinger, J.P., Arvidson, R.E., Bell, J.F., Calvin, W., Clark, B.C., Fike, D.A., Golombek, M., Greeley, R., Haldemann, A., Herkenhoff, K.E., and Jolliff, B.L. (2005) Stratigraphy and sedimentology of a dry to wet eolian depositional system, Burns formation, Meridiani Planum, Mars. Earth and Planetary Science Letters, 240, 11– 72.

Haskin, L.A. Wang, A., Jolliff, B.L., McSween, H.Y., Clark, B.C., Des Marais, D.J., McLennan, S.M., Tosca, N.J., Hurowitz, J.A., Farmer, J.D., and Yen, A. (2005) Water alteration of rocks and soils on Mars at the Spirit rover site in Gusev crater. Nature, 436, 66-70.

Johnson, J.R., Bell, J.F. III, Cloutis, E., Staid, M., Farrand, W.H., McCoy, T., Rice, M., Wang, A. and Yen, A. (2007) Mineralogic constraints on sulfur-rich soils from Pancam spectra at Gusev crater, Mars. Geophysical Research Letters, 34, L13202, doi:10.1029/2007GL9029894.

Kiely, A. and Klimesh, M. (2003) The ICER progressive wavelet image compressor. IPN Progress Report, 42, p.1-46.

Klingelhöfer, G., Morris, R.V., Bernhardt, B., Schröder, C., Rodionov, D.S., De Souza, P.A., Yen, A., Gellert, R., Evlanov, E.N., Zubkov, B., and Foh, J. (2004) Jarosite and Hematite at Meridiani Planum from Opportunity's Mössbauer Spectrometer. Science, 306, 1740-1745.

Lanza, N.L., Fischer, W.W., Wiens, R.C., Grotzinger, J., Ollila, A.M., Cousin, A., Anderson, R.B., Clark, B.C., Gellert, R., Mangold, N. and Maurice, S. (2014) High manganese concentrations in rocks at Gale crater, Mars. Geophysical Research Letters, 41, 5755-5763, doi:10.1002/2014GL060329.

Lane, M.D., Morris, R.V., and Christensen, P.R. (1999) Spectral behavior of hematite at visible/near infrared and mid-infrared wavelengths, 5th International Conference on Mars, abstract #6085.

Lane, M.D., Bishop, J.L., Dyar, M.D., King, P.L., Parente, M., and Hyde, B.C. (2008) Mineralogy of the Paso Robles soils on Mars. American Mineralogist, 93, 728-739.

McLennan, S.M., Bell, J.F. III, Calvin, W.M., Christensen, P.R., Clark, B.D., De Souza, P.A., Farmer, J., Farrand, W.H., Fike, D.A., Gellert, R. and Ghosh, A. (2005) Provenance and diagenesis of the Burns Formation, Meridiani Planum, Mars. Earth and Planetary Science Letters, 240, 95–121.

Ming, D.W., Mittlefehldt, D.W., Morris, R.V., Golden, D.C., Gellert, R., Yen, A., Clark, B.C., Squyres, S.W., Farrand, W.H., Ruff, S.W., and Arvidson, R.E. (2006), Geochemical and mineralogical indicators for aqueous processes in the Columbia Hills of Gusev crater, Mars. Journal of Geophysical Research-Planets, 111, E02S12, doi:10.1029/2005JE002560.

Ming, D.W., Gellert, R., Morris, R.V., Arvidson, R.E., Brueckner, J., Clark, B.C., Cohen, B.A., d'Uston, C., Economou, T., Fleischer, I., and Klingelhöfer, G. (2008) Geochemical properties of rocks and soils in Gusev Crater, Mars: Results of the Alpha Particle X-Ray Spectrometer from Cumberland Ridge to Home Plate, Journal of Geophysical Research-Planets. 113, E12S39, doi:10.1029/2008JE003195.

This is a preprint, the final version is subject to change, of the American Mineralogist (MSA)
Cite as Authors (Year) Title. American Mineralogist, in press.
(DOI will not work until issue is live.) DOI: http://dx.doi.org/10.2138/am-2016-5627

Morris, R.V., Klingelhöfer, G., Schröder, C., Rodionov, D.S., Yen, A., Ming, D.W., De Souza, P.A., Fleischer, I., Wdowiak, T., Gellert, R., and Bernhardt, B (2006) Mössbauer mineralogy of rock, soil, and dust at Gusev crater, Mars: Spirit's journey through weakly altered olivine basalt on the plains and pervasively altered basalt in the Columbia Hills. Journal of Geophysical Research-Planets. 111, E02S13, doi:10.1029/2005JE002584.

Morris, R. V., Klingelhöfer, G., Schröder, C., Fleischer, I., Ming, D.W., Yen, A.S., Gellert, R., Arvidson, R.E., Rodionov, D.S., Crumpler, L.S., and Clark, B.C. (2008) Iron mineralogy and aqueous alteration from Husband Hill through Home Plate at Gusev Crater, Mars: Results from the Mössbauer instrument on the Spirit Mars Exploration Rover. Journal of Geophysical Research-Planets. 113, E12S42, doi:10.1029/2008JE003201.

Nicolau, C., Reich, M., Lynne, B. (2014) Physico-chemical and environmental controls on siliceous sinter formation at the high-altitude El Tatio geothermal field, Chile. Journal of Volcanology and Geothermal Research, 282, 60-76.

Noe Dobrea, E.Z., Wray, J.J., Calef, F.J., Parker, T.J., and Murchie, S.L. (2012) Hydrated minerals on Endeavour Crater’s rim and interior, and surrounding plains: New insights from CRISM data. Geophysical Research Letters, 39, doi:10.1029/2012GL053180.

Potter, R.M. and Rossman, G.R. (1979) Mineralogy of manganese dendrites and coatings. American Mineralogist, 64, 1219-1226.

Reid, R.J., Smith, P.H., Lemmon, M., Tanner, R., Burkland, M., Wegryn, E., Weinberg, J., Marcialis, R., Britt, D.T., Thomas, N., and Kramm, R. (1999) Imager for Mars Pathfinder (IMP) image calibration. Journal of Geophysical Research-Planets, 104, 8907-8926.

Rice, M.S., Bell, J.F. III, Cloutis, E.A., Wang, A., Ruff, S.W., Craig, M.A., Bailey, D.T., Johnson, J.R., de Souza, P.A., and Farrand, W.H. (2010) Silica-rich deposits and hydrated minerals at Gusev Crater, Mars: Vis-NIR spectral characterization and regional mapping. Icarus, 205, 375-395.

Rice, M.S., Bell, J.F. III, Cloutis, E.A., Wray, J.J., Herkenhoff, K.E., Sullivan, R., Johnson, J.R., and Anderson, R.B. (2011) Temporal observations of bright soil exposures at Gusev crater, Mars. Journal of Geophysical Research-Planets, 116, E00F14, doi:10.1029/2010JE003683.

Rice, M.S., Cloutis, E.A., Bell, J.F. III, Bish, D.L., Horgan, B.H., Mertzman, S.A., Craig, M.A., Renaut, R.W., Gautason, B., and Mountain, B. (2013) Reflectance spectra diversity of silica-rich materials: Sensitivity to environment and implications for detections on Mars. Icarus, 223, 499–533. doi:10.1016/j.icarus.2012.09.021.

Rieder, R., Gellert, R., Anderson, R.C., Brückner, J., Clark, B.C., Dreibus, G., Economou, T., Klingelhöfer, G., Lugmair, G.W., Ming, D.W., and Squyres, S.W. (2004) Chemistry of Rocks and Soils at Meridiani Planum from the Alpha Particle X-ray Spectrometer. Science, 306, 1746-1749.

Ruff, S.W., Christensen, P.R., Glotch, T.D., Blaney, D.L., Moersch, J.E., and Wyatt, M.B. (2008) The mineralogy of Gusev crater and Meridiani Planum derived from the Miniature Thermal Emission Spectrometers on the Spirit and Opportunity rovers. In J.F. Bell III, Ed., The Martian Surface: Composition, Mineralogy, and Physical Properties, p. 315-338. Cambridge University Press, New York.

Ruff, S.W., Farmer, J.D., Calvin, W.M., Herkenhoff, K.E., Johnson, J.R., Morris, R.V., Rice, M.S., Arvidson, R.E., Bell, J.F. III, Christensen, P.R., and Squyres, S.W. (2011) Characteristics, distribution, origin, and significance of opaline silica observed by the Spirit rover in Gusev crater, Mars. Journal of Geophysical Research- Planets, 116, no. E7, E00F23, doi:10.1029/2010JE003767.

Ruff, S.W. (2015) New observations reveal a former hot spring environment with high habitability and preservation potential in Gusev crater, Mars. 46th Lunar and Planetary Science Conference, abstract #1613.

Schmidt, M.E., Farrand, W.H., Johnson, J.R., Schröder, C., Hurowitz, J.A., McCoy, T.J., Ruff, S.W., Arvidson, R.E., Des Marais, D.J., Lewis, K.W., and Ming, D.W. (2009) Spectral mineralogical, and geochemical variations across Home Plate, Gusev Crater, Mars indicate high and low temperature alteration. Earth and Planetary Science Letters, 281, 258-266.

Singer, R.B. (1982) Spectral evidence for the mineralogy of high-albedo soils and dust on Mars. Journal of Geophysical Research, 87, 10159-10168.

Sohl-Dickstein, J., Johnson, J.R., Grundy, W.M., Guinness, E., Graff, T., Shepard, M.K., Arvidson, R.E., Bell, J.F. III, Christensen, P.R., and Morris, R.V. (2005) Modeling Visible/Near-Infrared photometric properties of dustfall on a known substrate. Lunar and Planetary Science Conference XXXVI, abstract #2235.

Squyres, S.W., Arvidson, R.E., Blaney, D.L., Clark, B.C., Crumpler, L.S., Farrand, W.H., Gorevan, S., Herkenhoff, K.E., Hurowitz, J., Kusack, A., and others (2006) The Rocks of the Columbia Hills. Journal of Geophysical Research- Planets, 111, E02S11, 10.1029/2005JE002562.

Squyres, S.W., Aharonson, O., Clark, B.C., Cohen, B.A., Crumpler, L., De Souza, P.A., Farrand, W.H., Gellert, R., Grant, J., Grotzinger, J.P., and Haldemann, A.F.C. (2007) Pyroclastic activity at Home Plate in Gusev Crater, Mars. Science, 316, 738-742.

Squyres, S.W., Arvidson, R.E., Ruff, S., Gellert, R., Morris, R.V., Ming, D.W., Crumpler, L., Farmer, J.D., Des Marais, D.J., Yen, A., and McLennan, S.M. (2008) Detection of silica-rich deposits on Mars. Science, 320, 1063-1067.

Squyres, S.W., Arvidson, R.E., Bell, J.F. III, Calef, F., Clark, B.C., Cohen, B.A., Crumpler, L.A., De Souza, P.A., Farrand, W.H., Gellert, R., and Grant, J. (2012) Ancient impact and aqueous processes at Endeavour crater, Mars. Science, 336, 570-576.

Vaniman, D. T., Bish, D.L., Ming, D.W., Bristow, T.F., Morris, R.V., Blake, D.F., Chipera, S.J., Morrison, S.M., Treiman, A.H., Rampe, E.B. and Rice, M.S. (2014) Mineralogy of a mudstone at Yellowknife Bay, Gale Crater, Mars. Science, 343, doi:10.1126/science1243480.

Wang, A., Haskin, L.A., Squyres, S.W., Jolliff, B.L., Crumpler, L., Gellert, R., Schröder, C., Herkenhoff, K., Hurowitz, J., Tosca, N.J. ,and Farrand, W.H. (2006) Sulfate deposition in subsurface regolith in Gusev crater, Mars. Journal of Geophysical Research- Planets. 111, E02S17, doi:10.1029/2005JE002513.

Wang, A., Bell, J.F. III, Li, R., Johnson, J.R., Farrand, W.H., Cloutis, E.A., Arvidson, R.E., Crumpler, L., Squyres, S.W., McLennan, S.M., and Herkenhoff, K.E. (2008) Light-toned salty soils and coexisting Si-rich species discovered by the Mars Exploration Rover Spirit in Columbia Hills. Journal of Geophysical Research- Planets, 113, E12S40, doi:10.1029/2008JE003126.

Wang, A., and Ling, Z.C. (2011) Ferric sulfates on Mars: A combined mission data analysis of salty soils at Gusev crater and laboratory experimental investigations. Journal of Geophysical Research- Planets, 116, E00F17, doi:10.1029/2010JE003665.

Wellington, D.F., Bell, J.F. III, Johnson, J.R., Kinch, K.M., Rice, M.S., and Fraeman, A.A. (2016) Visible and near infrared spectra of select high-interest science targets within Gale Crater, observed by MSL Mastcam. American Mineralogist, in press.

Wray, J.J., Noe Dobrea, E.Z., Arvidson, R.E., Wiseman, S.M., Squyres, S.W., McEwen, A.S., Mustard, J.F., and Murchie, S.L. (2009) Phyllosilicates and sulfates at Endeavour Crater, Meridiani Planum, Mars. Geophysical Research Letters, 36, L21201, doi:10.1029/2009GL040734.

Yen, A. S., Morris, R.V., Clark, B.C., Gellert, R., Knudson, A.T., Squyres, S., Mittlefehldt, D.W., Ming, D.W., Arvidson, R., McCoy, T. and Schmidt, M. (2008) Hydrothermal processes at Gusev Crater: An evaluation of Paso Robles Class soil. Journal of Geophysical Research-Planets, 113, E06S10, doi:10.1029/2007JE002978

Figure Captions

Figure 1. A. L357 (673, 535, 432 nm) enhanced color view of RATed El Capitan from Opportunity sol 37 (sequence P2532). **B**. Pancam spectrum of RAT grind interior (red) vs. a library spectrum (from the USGS spectral library, Clark et al., 2007) of red hematite (black, reflectance values of library spectrum divided by 2).

Figure 2. A. Library reflectance spectra of coarsely crystalline hematite. **B**. Average of blueberries from scenes P2556 from sol 45 and from P2585 from sol 51.

Figure 3. Full spectral resolution library spectra (Clark et al., 2007; PDS spectral library) of red, dark red, and gray hematite over the Pancam spectral range of 430 to 1010 nm.

Figure 4. Sol 33 P2589 L357 (673, 535, 432 nm) stretched color composite of target “Cathedral Dome”. Blue arrow indicates the buff-colored “HFS” Burns formation color unit of Farrand et al. (2007) and the black arrow indicates the purple-colored “LFS” Burns formation color unit.

Figure 5. A. Representative Pancam spectra (denoted by sol number with the prefix of “B” and Pancam sequence number of “P” plus 4 digits) of Burns formation “LFS” (or purple-colored in typically used color composites) surfaces. **B**. Representative Grasberg formation surface spectra (after Farrand et al., 2014).

Figure 6. Plots of spectral parameters discriminating Burns and Grasberg formations. **A**. Fitted NIR band minimum vs. 535 nm band depth (after Farrand et al., 2014). **B**. 754 to 1009 nm slope vs. 535 nm band depth.

Figure 7. Subsection of sol 3567 P2535 L357 (673, 535, 432 nm) composite shows overturned rocks Pinnacle Island (inside green circle) and Stuart Island (inside red circle). Both have the light and dark-toned coatings.

Figure 8. A. Dark coating on Pinnacle Island. **B**. Desert varnish spectra from USGS spectral library (Clark et al., 2007). The ANP90-14 sample is a desert varnish coating on a sandstone and GDS78 is desert varnish coating on rhyolite and quartz cobbles.

Figure 9. A. L357 (673, 535, 432 nm) view of target Monjon (Sol 3419 P2559). Blue coating indicated by arrow. **B**. R731 (1009, 803, 436 nm) view of Monjon. **C**. 535 nm band depth view of Monjon. White arrow indicates low 535 nm band depth associated with coating.

Figure 10. Spectra of blue coatings on Grasberg formation exposures observed on sols 3739 and 3419.

Figure 11. A. L357 (673, 535, 432 nm) composite of Spirit sol 721 P2538 view of Arad soils at the Dead Sea site. Red polygon and circle indicate spectral extraction region for “yellow” soil in spectral plot of **Fig. 11B** and blue polygon and circle indicate spectral extraction region for

"white" soil in spectral plot of **Fig. 11B.** **B**. White and yellow soils from sol 721 P2538 Arad observation. Spectra extracted from sites noted in **Fig. 11A.**

Figure 12 A. Sol 471 P2538 Arad white soil. **B**. Library spectra, convolved to Pancam bandpasses of best match (in mixtures) spectra from Johnson et al. (2007).

Figure 13. Opportunity sol 2769 P2574 L357 (673, 535, 432 nm) view of gypsum vein "Homestake" in Cape York bench.

Figure 14. Library spectra (Cloutis et al., 2006; Clark et al., 2007) of calcium sulfate minerals at full spectral resolution over the Pancam spectral range (A) and convolved to Pancam bandpasses (B).

Figure 15. Plot of 754 to 1009 nm slope vs. 535 nm band depth for gypsum veins observed on the bench of Cape York vs. those observed in the Matijevic formation on Matijevic Hill.

Figure 16. **A**. Pinnacle Island bright coating spectrum. **B**. Library spectra (Clark et al., 2007) of Mg sulfate minerals epsomite and kieserite.

Figure 17. Silica-rich materials in the Inner Basin of the Columbia Hills of Gusev crater, discovered by Spirit. **A**. Pancam L357 (673, 535, 432 nm) composite of the Innocent Bystander nodular outcrop (sol 1294, P2581). **B.** Pancam L357 composite of the Gertrude Weise soil (sol 1187, P2533), which contains ~98% SiO_2 (Squyres et al., 2008). The width of the wheel track is

~16 cm. **C.** Pancam relative reflectance spectra of silica-rich targets (see Rice et al., 2010 for further discussion). All spectra exhibit a relatively flat near-infrared profile (864 to 934 nm) and a characteristic downturn in the longest-wavelength filter (1009 nm) due to H_2O and/or OH absorptions near ~1000 nm. Figure modified from Rice et al., (2013).

Figure 18. A. Sol 3090 P2571 L357 (673, 535, 432 nm) composite of Whitewater Lake outcrop showing the gray-toned Azilda RAT grind spot. **B.** Sol 3098 P2580 L357 view of the RAT-brushed Chelmsford dark-toned coatings target. **C**. Sol 3262 P2579 L357 composite of Lihir/Esperance boxwork structure pre-RAT grind. The Esperance target is circled.

Figure 19. A. Matijevic formation Whitewater Lake matrix spectra. **B**. Matijevic formation Whitewater Lake dark coating spectra.

Figure 20. Representative boxwork fracture fill spectra of targets Esperance and Lihir plus a piece of boxwork fracture fill broken by the rover’s wheels.

Figure 21. A. 754 to 1009 nm slope vs. 535 nm band depth for gypsum veins and boxwork fracture fills. **B**. Fitted reflectance peak positions vs. 535 nm band depth for gypsum veins and boxwork fracture fills.

Figure 22. Comparison of spectra of Esperance light-toned “as-is” surface to that of a broken Si-rich nodule surface on the Innocent Bystander target.

Figure 23. R6/R7 ratio vs. 754 to 1009 nm slope of Home Plate Eastern Valley silica nodules (values from sol 1279 and 1294 views of broken surfaces on Innocent Bystander) compared with Lihir and Esperance (values from sols 3230 (Lihir) and 3262 (Esperance)).

Tables

Name	*Center λ (nm)*	*Bandpass (nm)*	*Description*
L1	739	338	Empty
L2	753	20	Geology, Red stereo left
L3	673	16	Geology
L4	601	17	Geology
L5	535	20	Geology
L6	482	30	Geology
L7	432	32	Geology, Blue stereo left
L8	440	20	Solar neutral density
R1	436	37	Geology, Blue stereo right
R2	754	20	Geology, Red stereo right
R3	803	20	Geology
R4	864	17	Geology
R5	904	26	Geology
R6	934	25	Geology
R7	1009	38	Geology
R8	880	20	Solar neutral density

Table 1. Pancam Filters

Parameter	*Formula*	*Utility*
482 to 673 nm slope	1000*((R673 –R482)/191)	Gauge of Fe oxidation
535 nm band depth	1-(R535/((0.57*R432)+(0.43*R673)))	Gauge of development of ferric oxides
601 nm band depth	1-(R601/((0.52*R535)+(0.48*R673)))	Assess convexity near 600 nm
803 nm / 904 nm	R803/R904	Indicator of strength of NIR absorption band
803 nm / 1009 nm	R803/R1009	Help distinguish between olivine and pyroxene dominated lithologies
904 nm band depth	1-(R904/((0.51*R803)+(0.49*R1009)))	Assess depth of NIR absorption band
754 to 1009 nm slope	1000*((R1009-R754)/255)	Gauge of hematite development; indicator of pyroxene, olivine.
934 to 1009 nm slope	1000*((R1009-R934)/75)	Indicator of H_2O overtone band
Fitted reflectance peak position	Maximum of 5^{th} degree polynomial fitted to bands from 535 to 904 nm	Gauge of Fe oxidation
Fitted NIR band minimum position	Minimum of 3^{rd} degree polynomial fitted to bands from 864 to 1009 nm	Distinguish between Fe-bearing phases

Table 2. Pancam Spectral Parameters (note that the factor of 1000 in slope calculations is only a scaling factor). Notation such as “R673” refers to the reflectance in the 673 nm band.

Figures

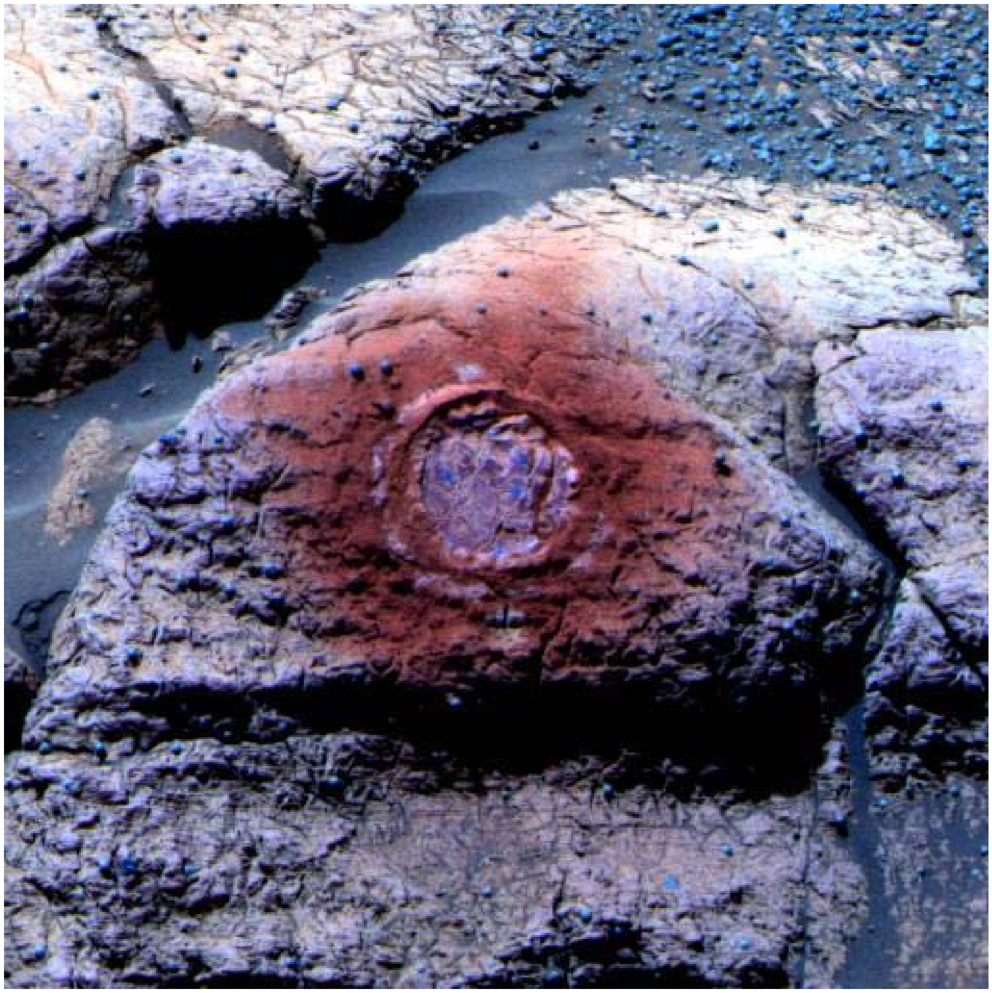

Figure 1A.

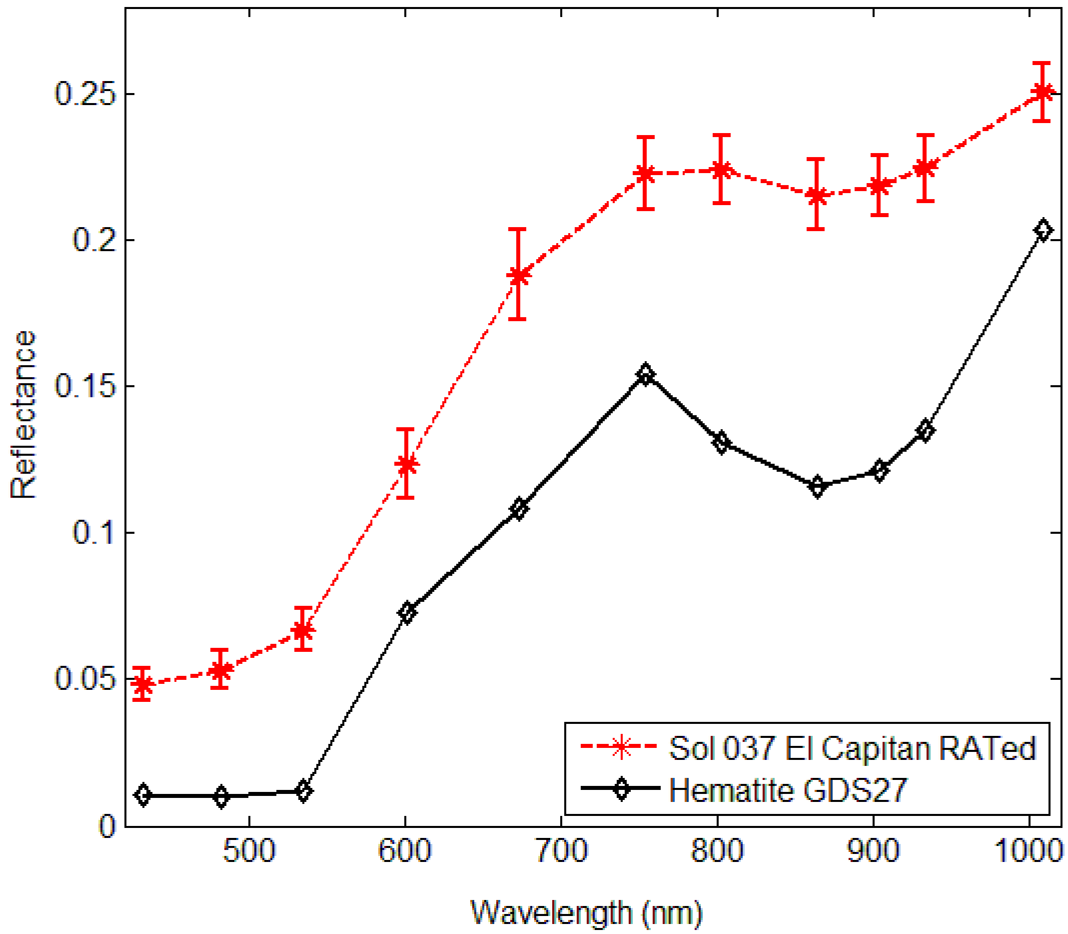
Reflectance
0.25
0.2
0.15
0.1
0.05
0
500
600
700
800
900
1000
Wavelength (nm)
Sol 037 El Capitan RATed
Hematite GDS27

Figure 1B.

This is a preprint, the final version is subject to change, of the American Mineralogist (MSA)
Cite as Authors (Year) Title. American Mineralogist, in press.
(DOI will not work until issue is live.) DOI: http://dx.doi.org/10.2138/am-2016-5627

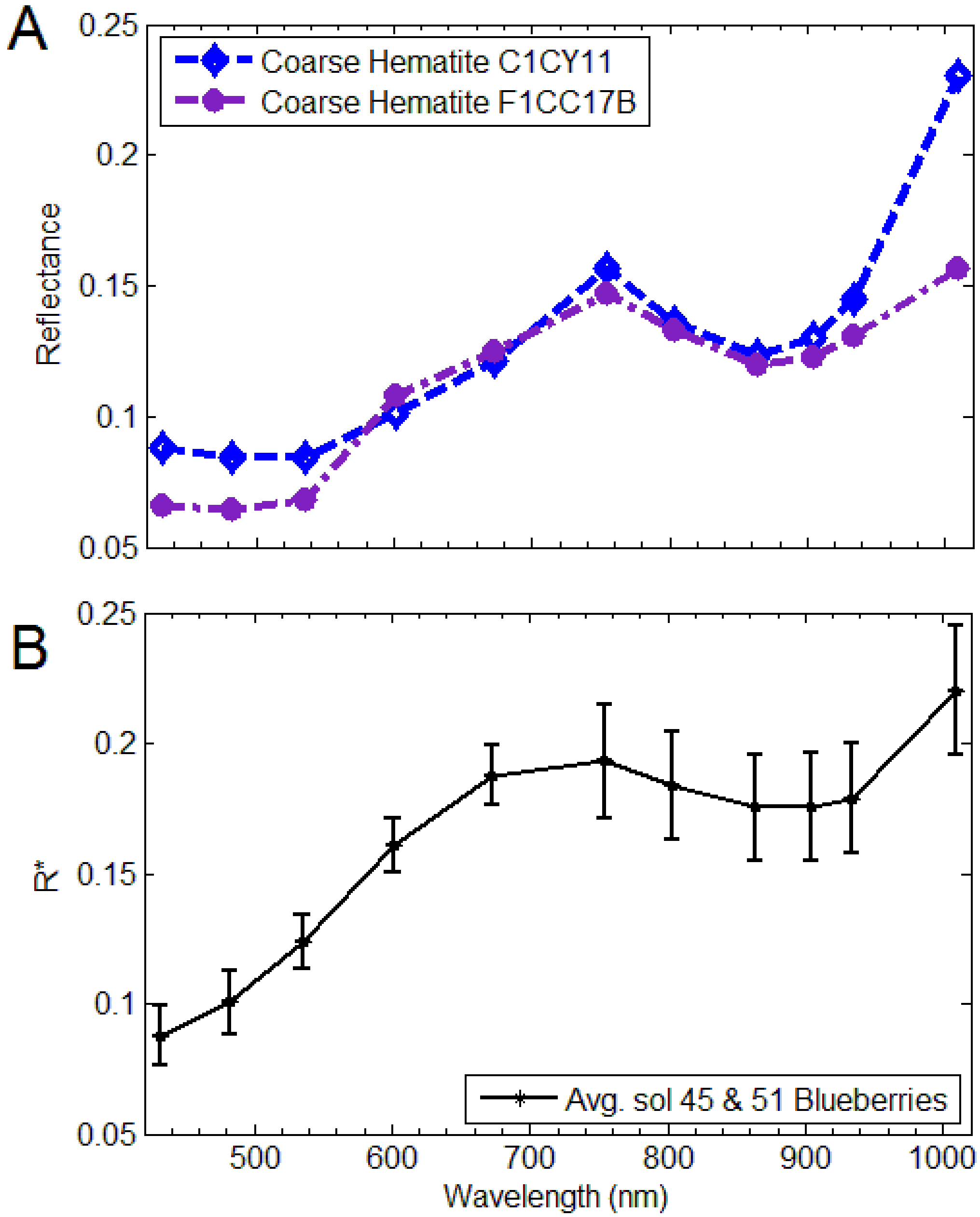

Figure 2.

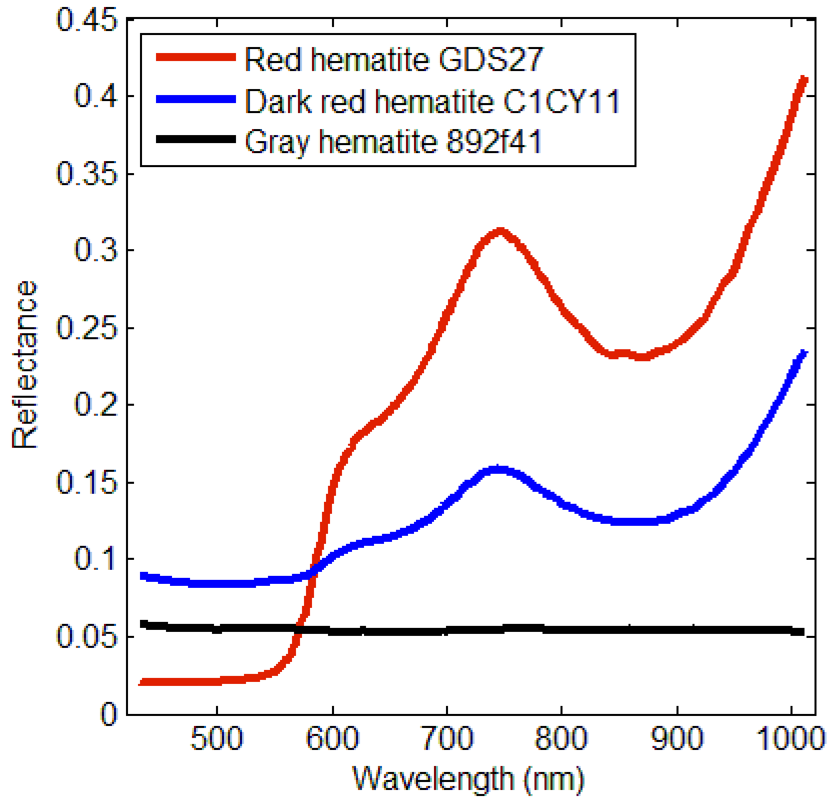

979

980 Figure 3.

This is a preprint, the final version is subject to change, of the American Mineralogist (MSA)
Cite as Authors (Year) Title. American Mineralogist, in press.
(DOI will not work until issue is live.) DOI: http://dx.doi.org/10.2138/am-2016-5627

981 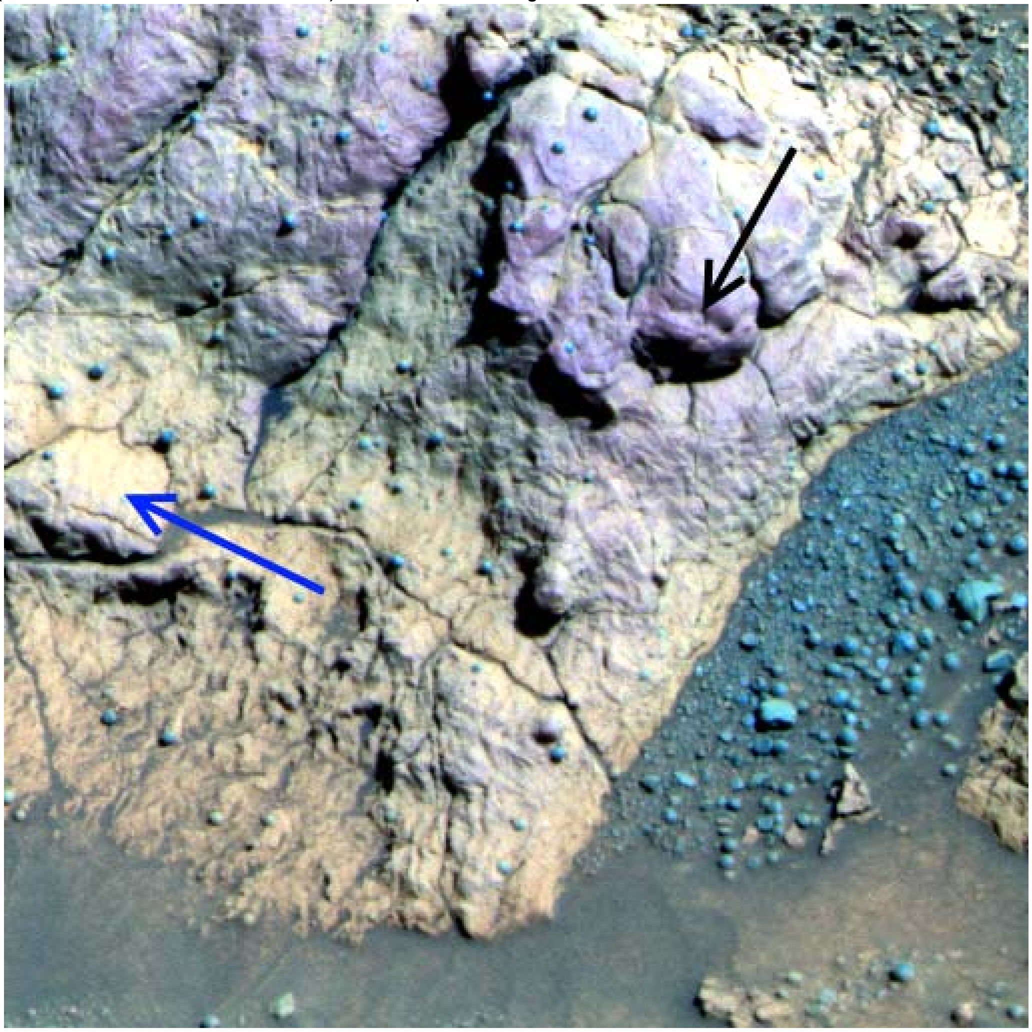

982 Figure 4.

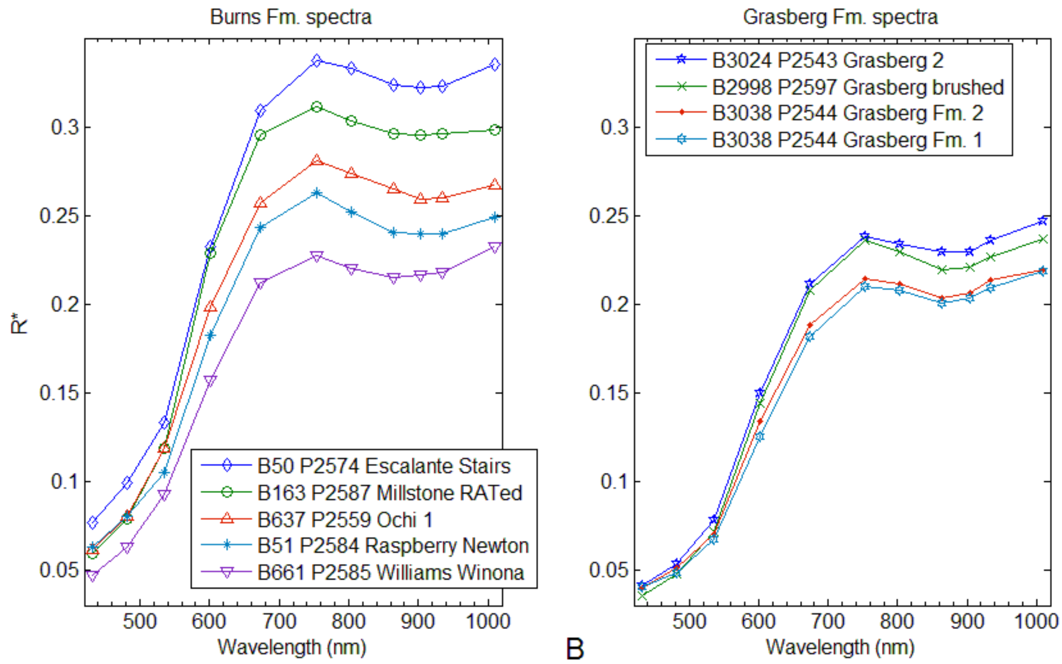

Figure 5.

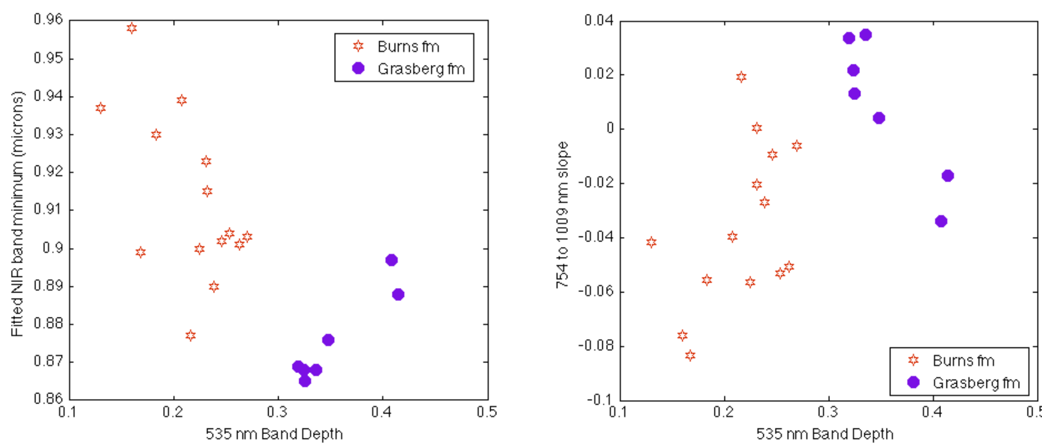

Figure 6.

987 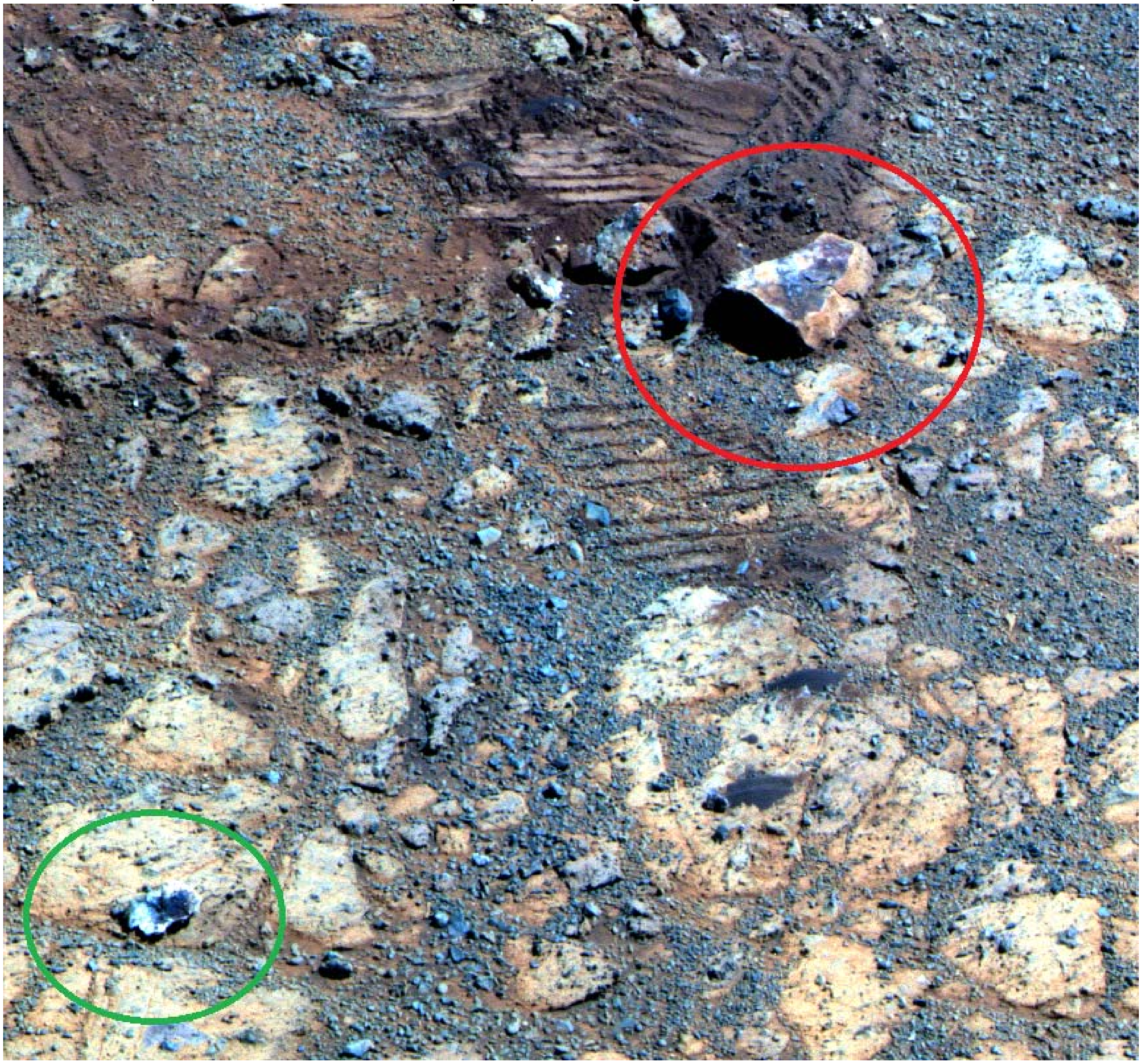

988 Figure 7.

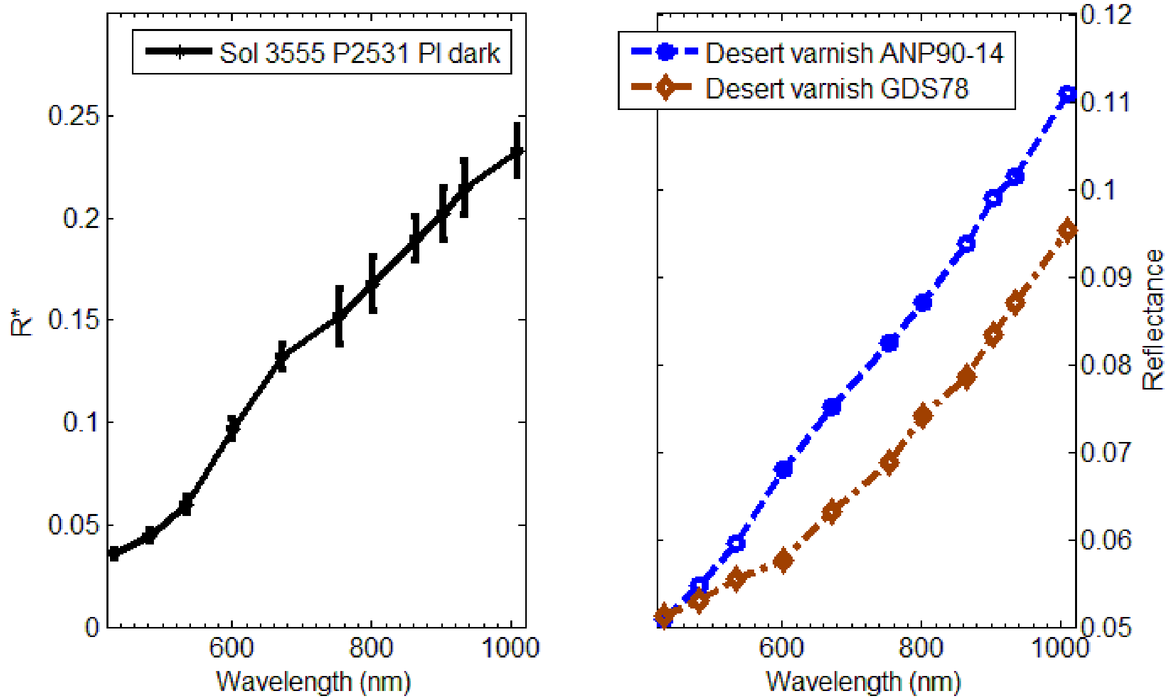

Figure 8.

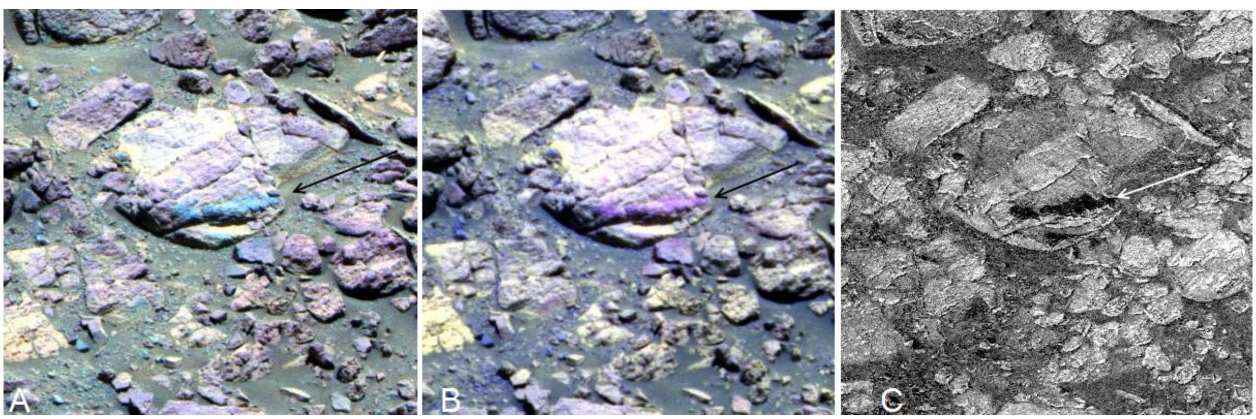

Figure 9.

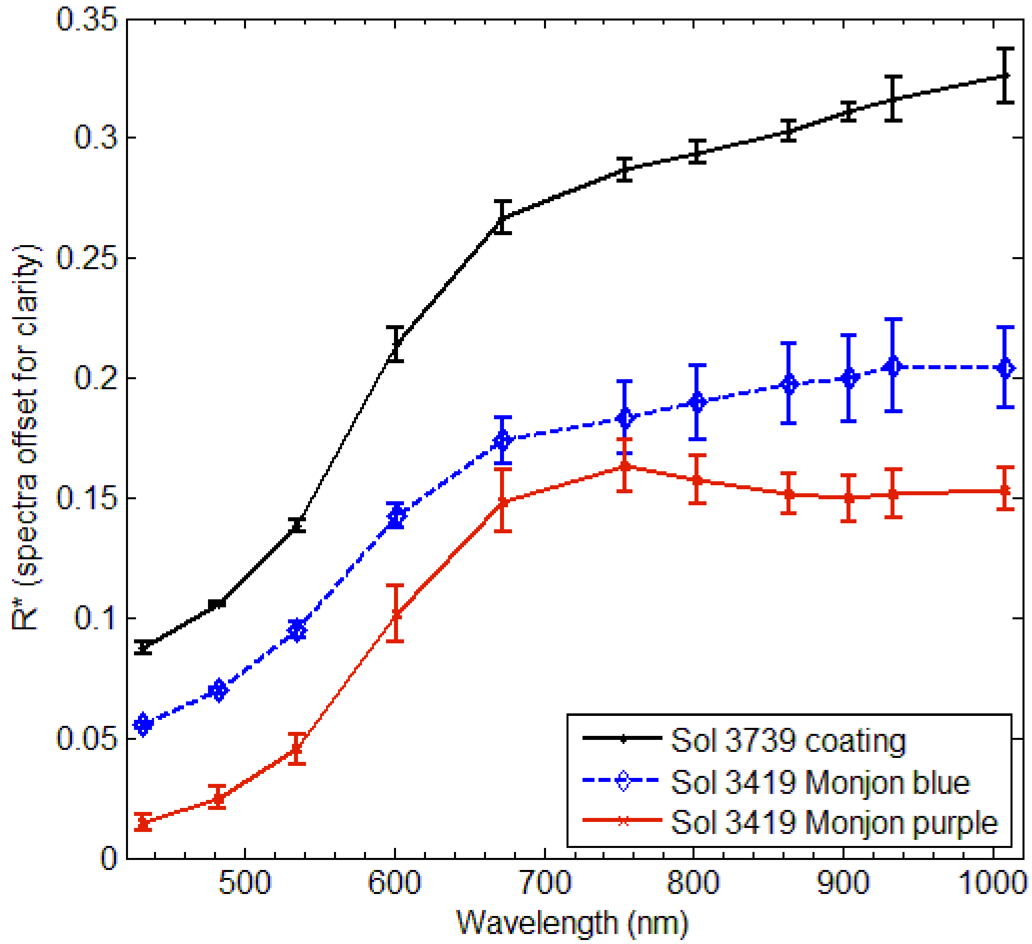

993

994 Figure 10.

Figure 11A.

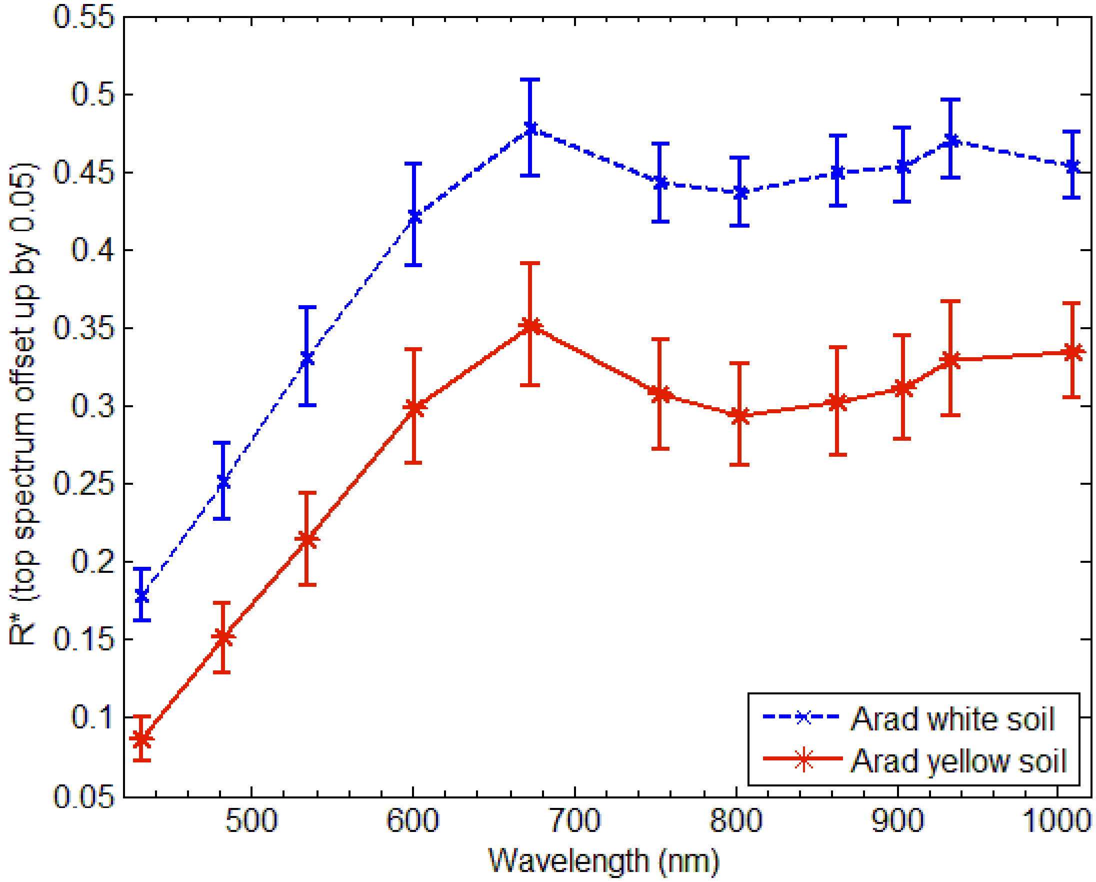

997

998 Figure 11B.

This is a preprint, the final version is subject to change, of the American Mineralogist (MSA)
Cite as Authors (Year) Title. American Mineralogist, in press.
(DOI will not work until issue is live.) DOI: http://dx.doi.org/10.2138/am-2016-5627

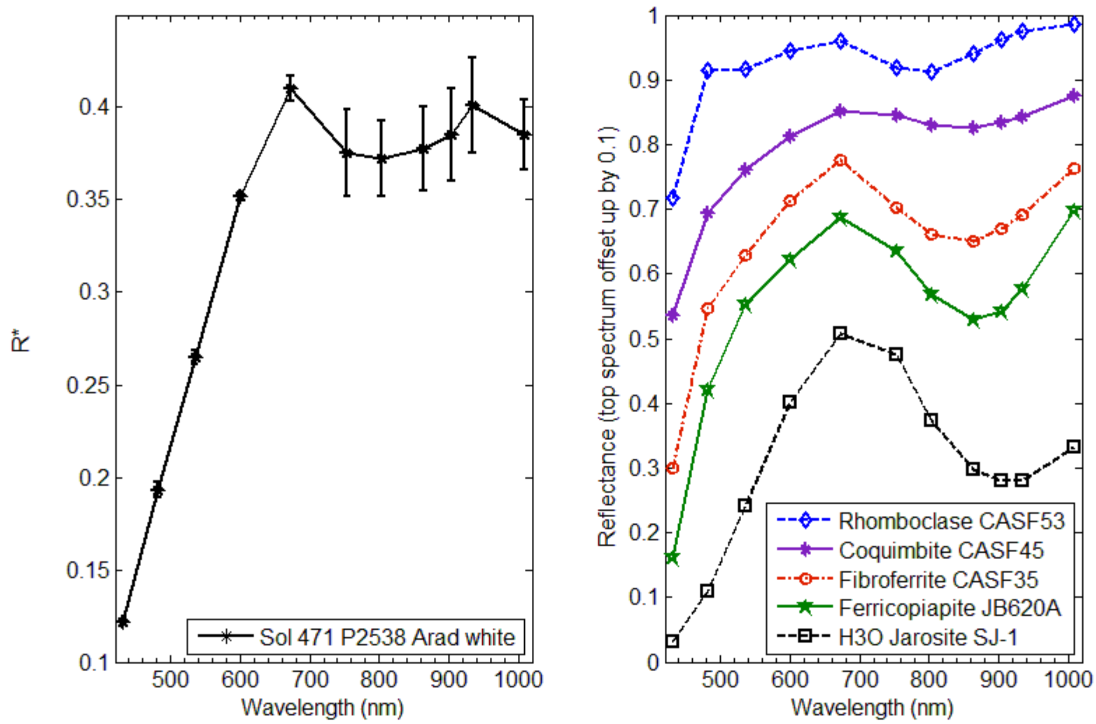

Figure 12.

Figure 13.

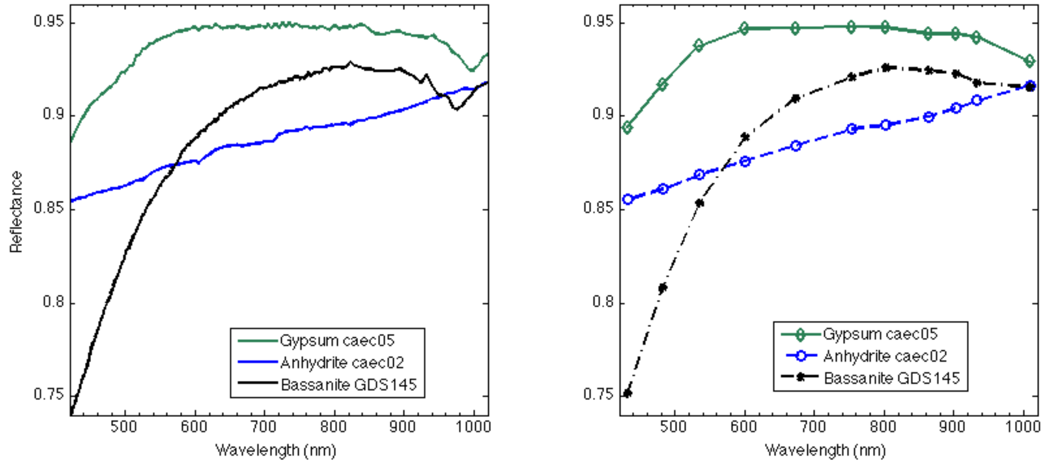

Figure 14.

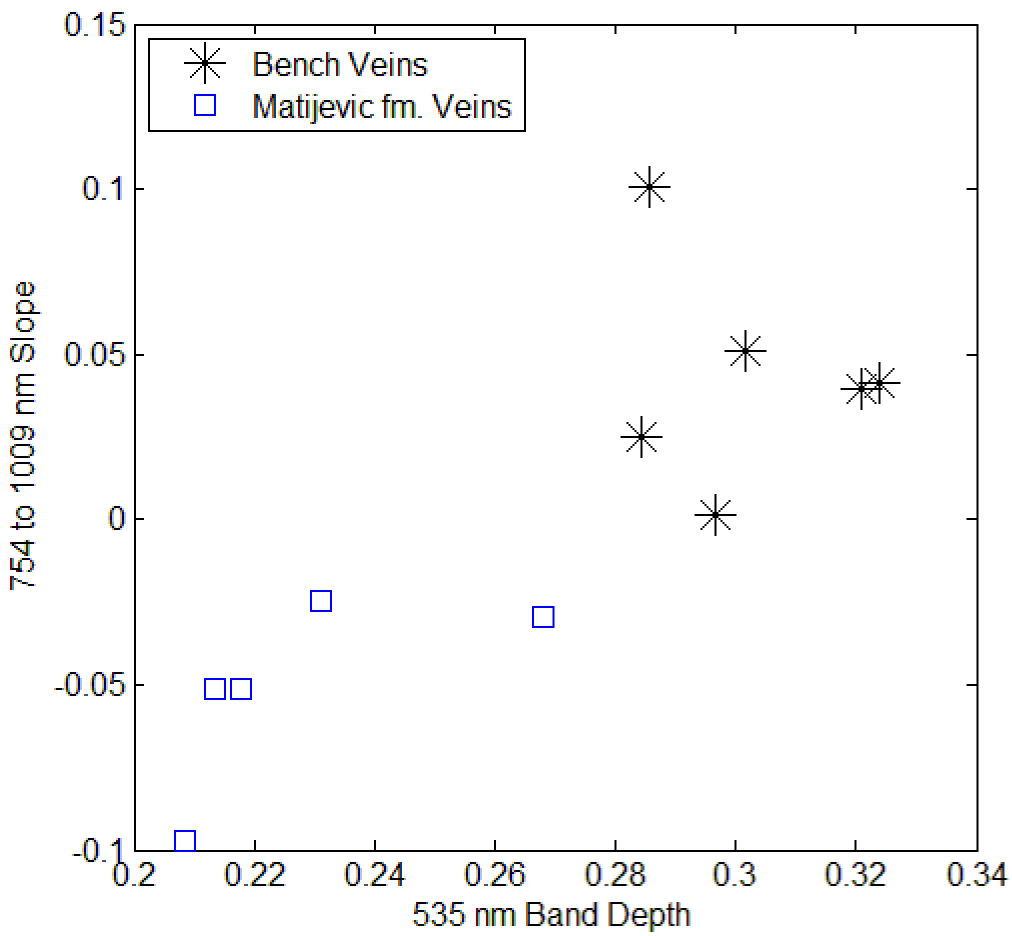

Figure 15.

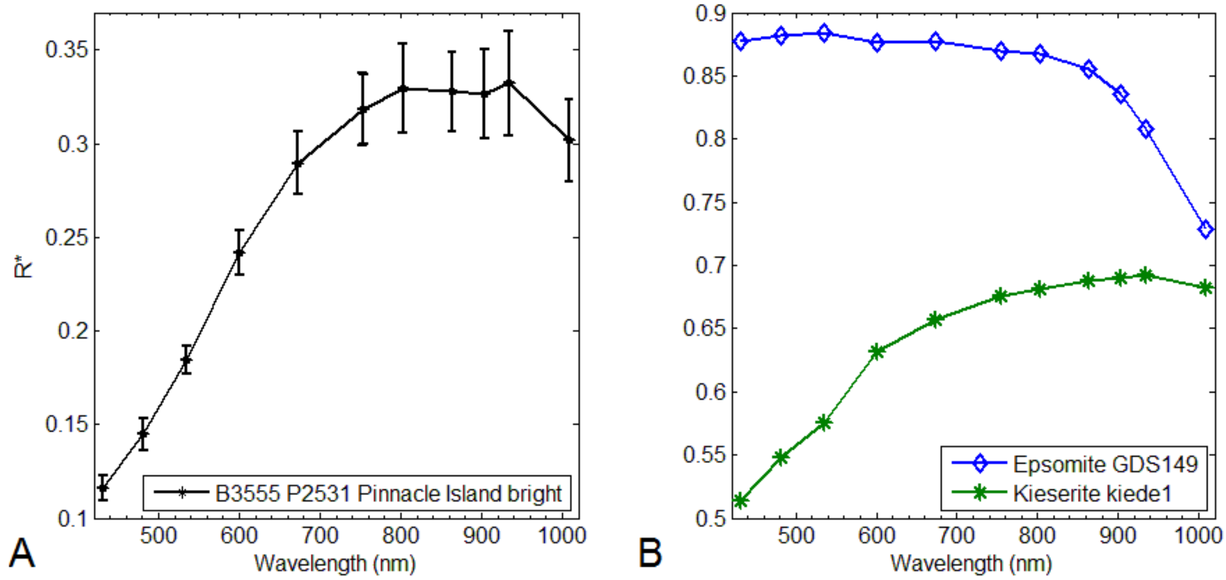
R*
B3555 P2531 Pinnacle Island bright
Wavelength (nm)
A
Epsomite GDS149
Kieserite kiede1
Wavelength (nm)
B

Figure 16.

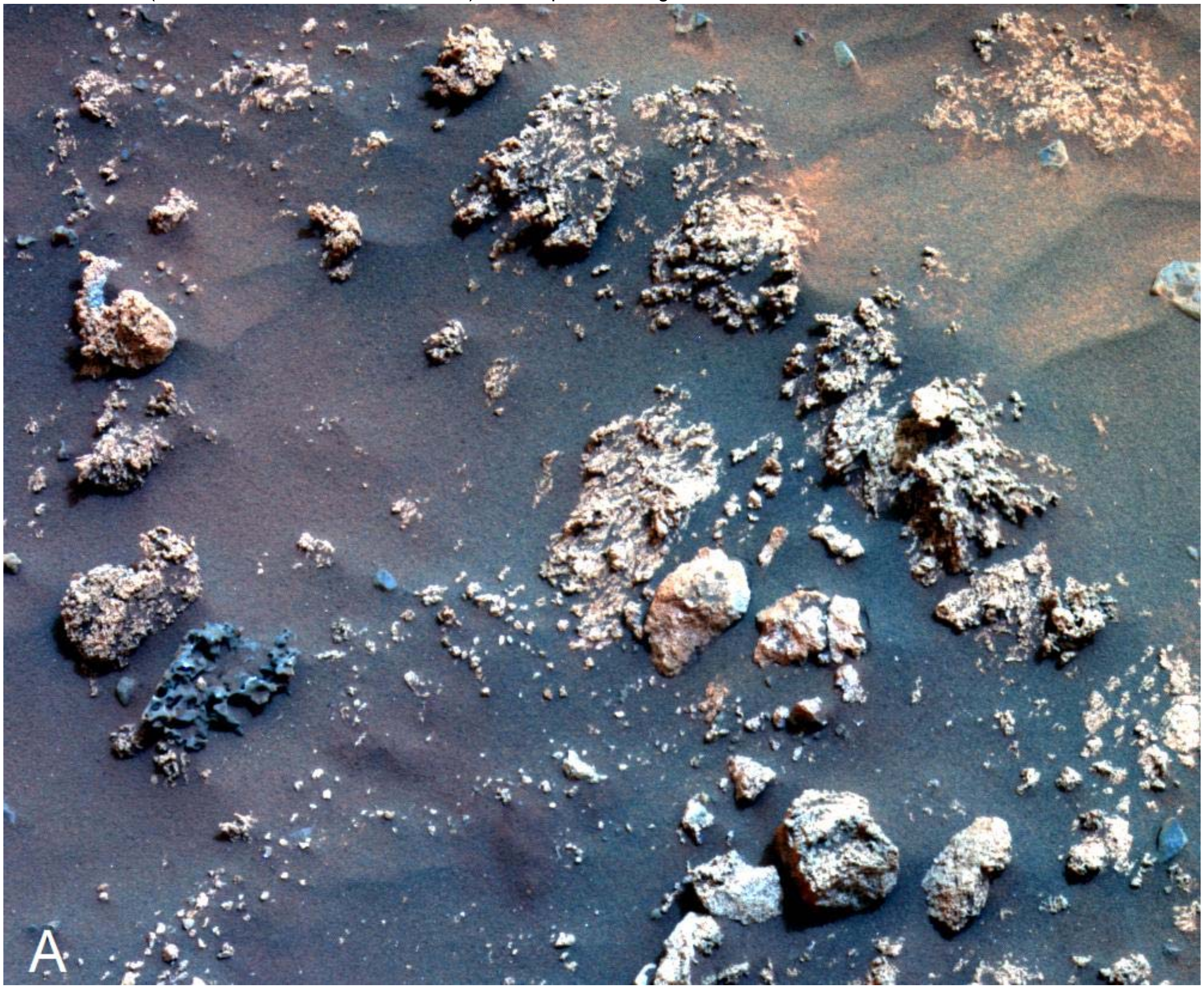

Figure 17A.

Figure 17B.

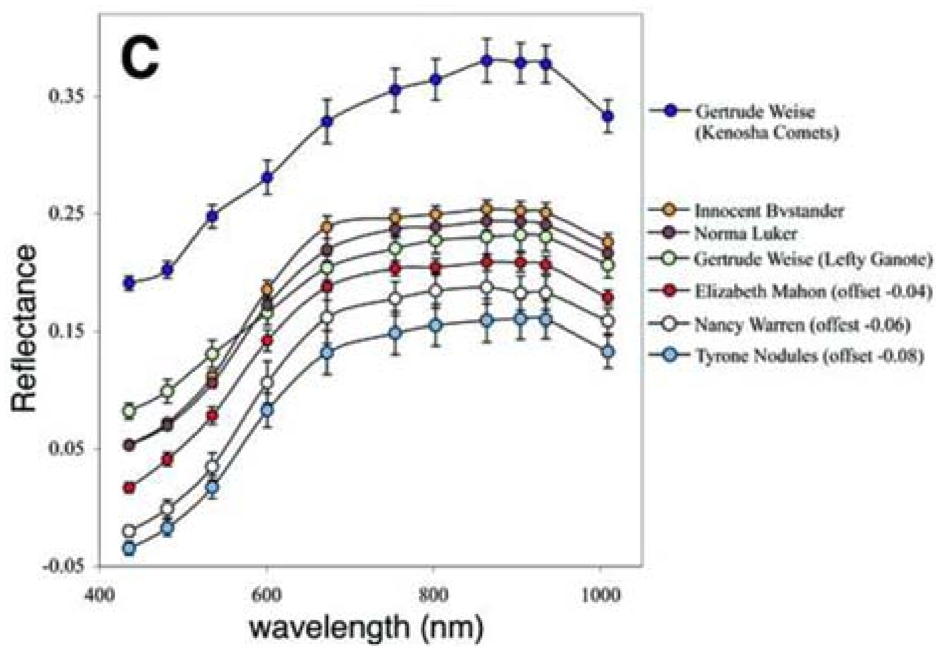

Figure 17C.

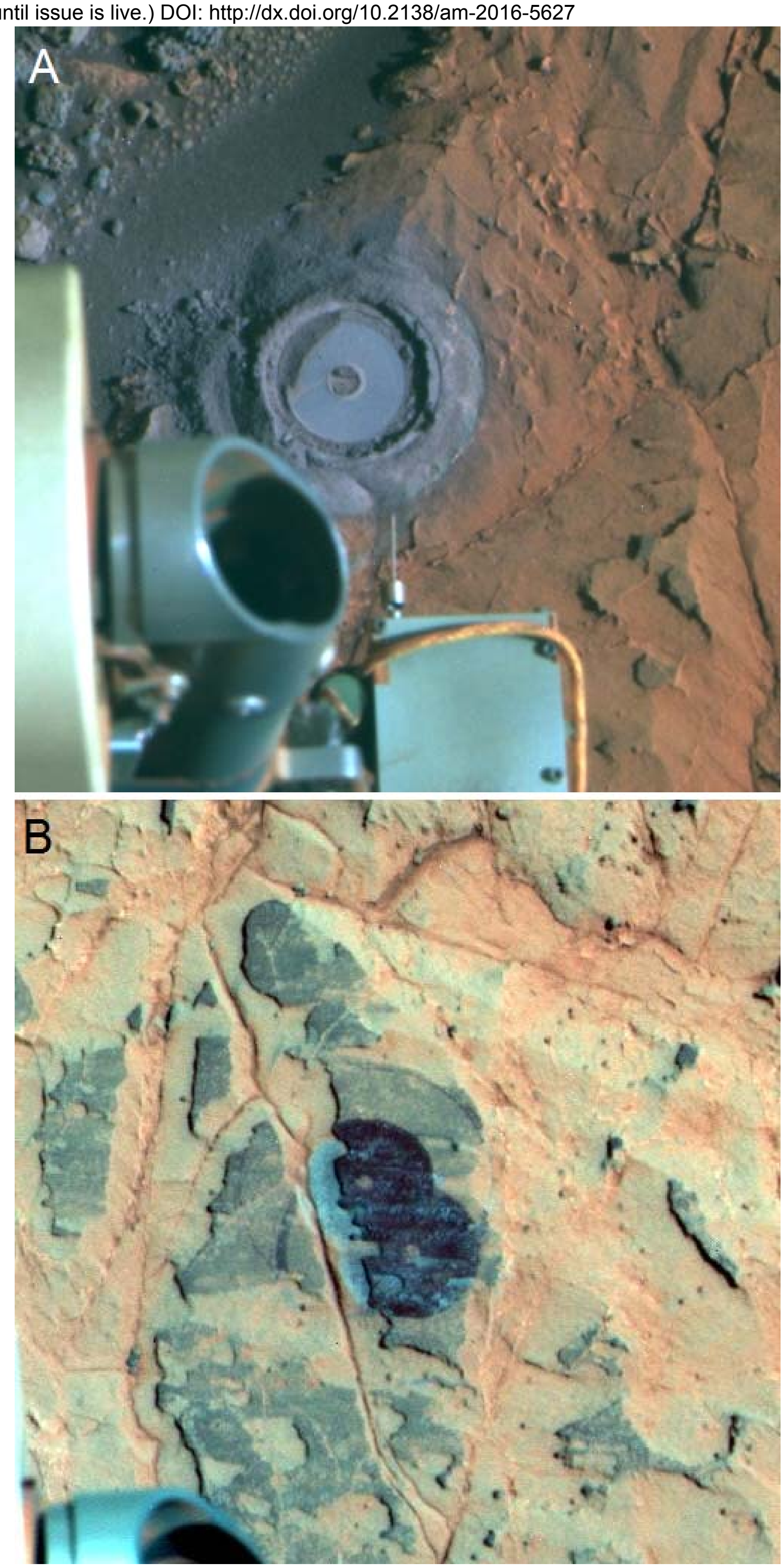

Figure 18 A and B.

Figure 18C.

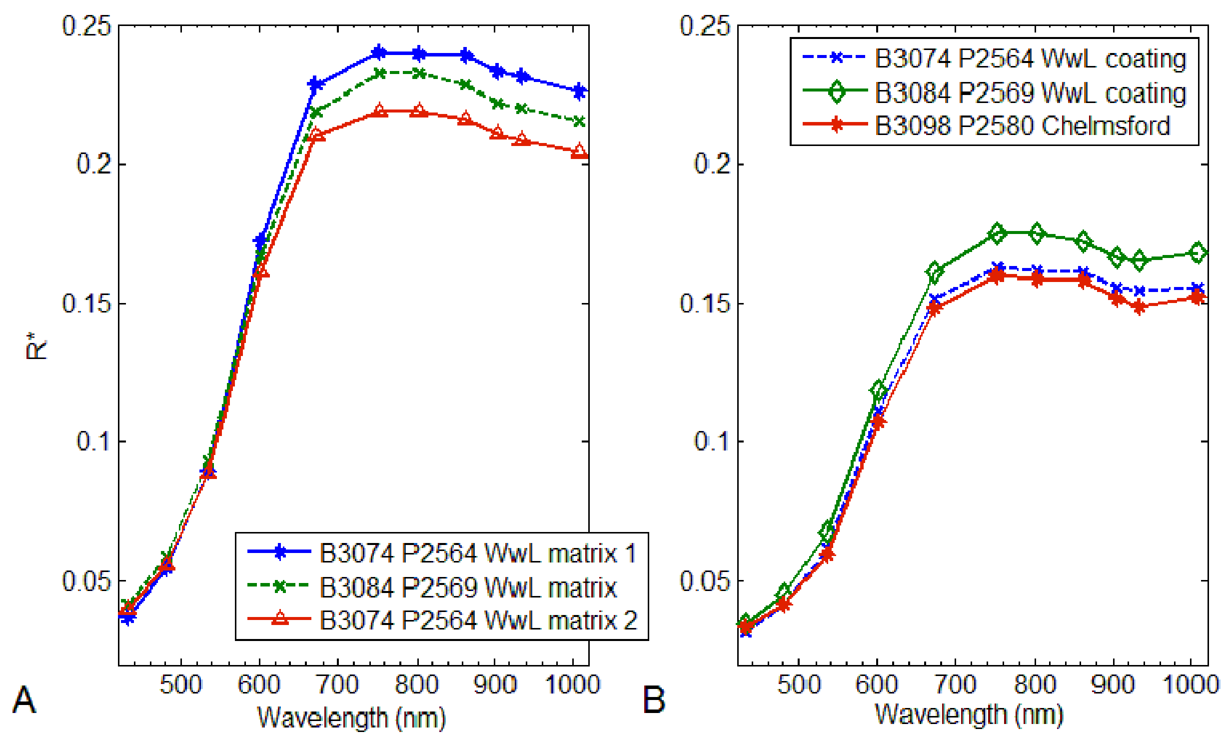

Figure 19.

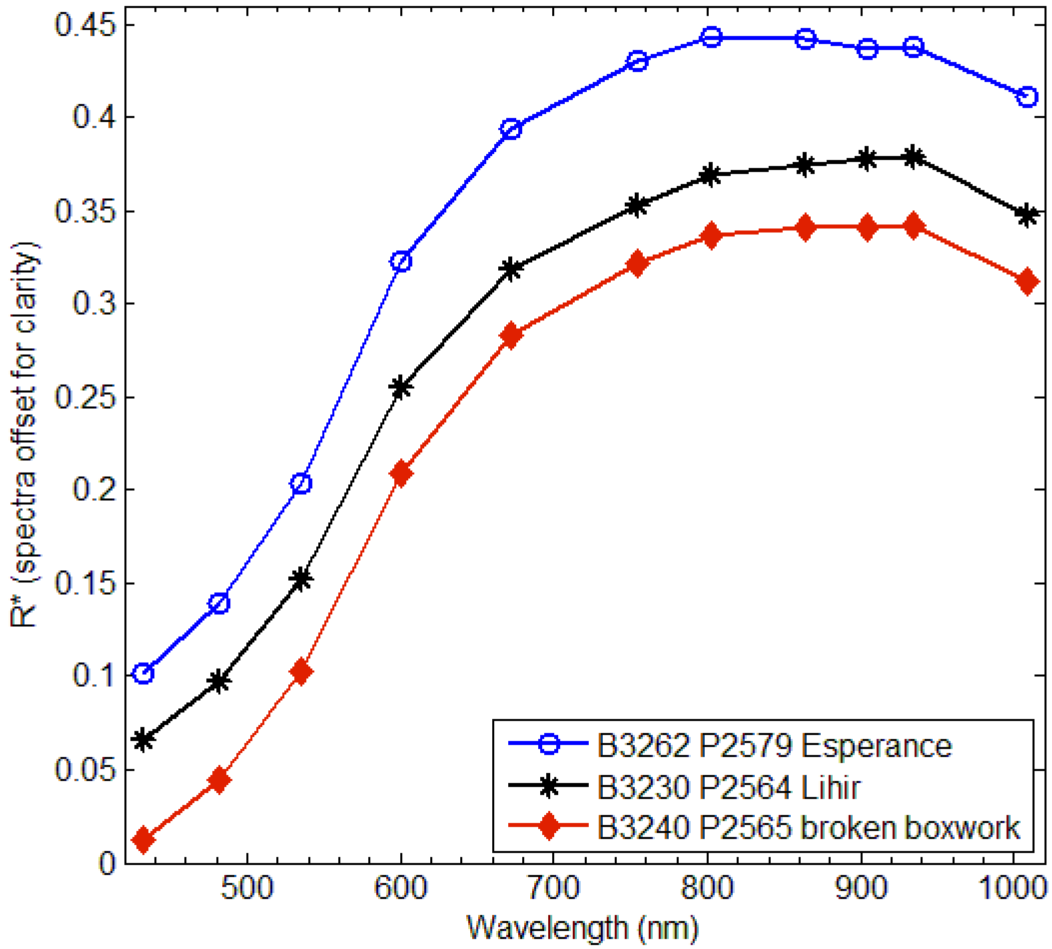

1021

1022 Figure 20.

This is a preprint, the final version is subject to change, of the American Mineralogist (MSA)
Cite as Authors (Year) Title. American Mineralogist, in press.
(DOI will not work until issue is live.) DOI: http://dx.doi.org/10.2138/am-2016-5627

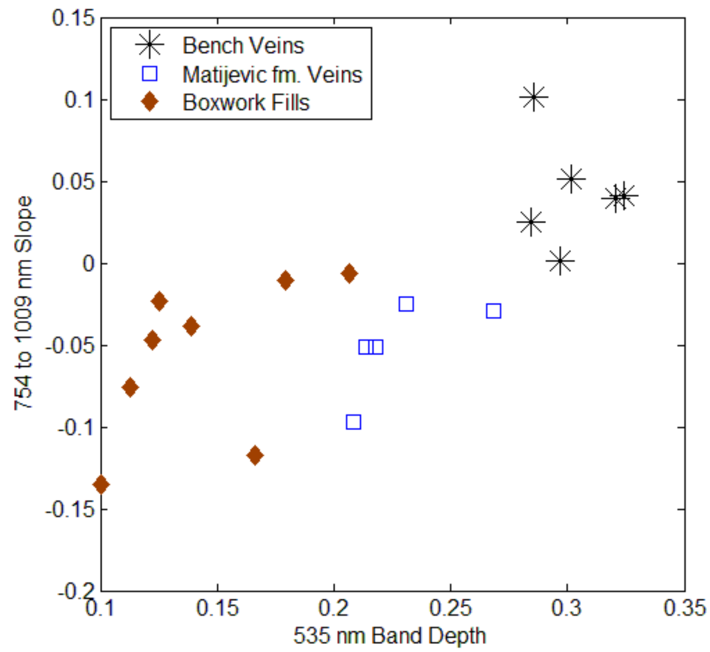

Figure 21A.

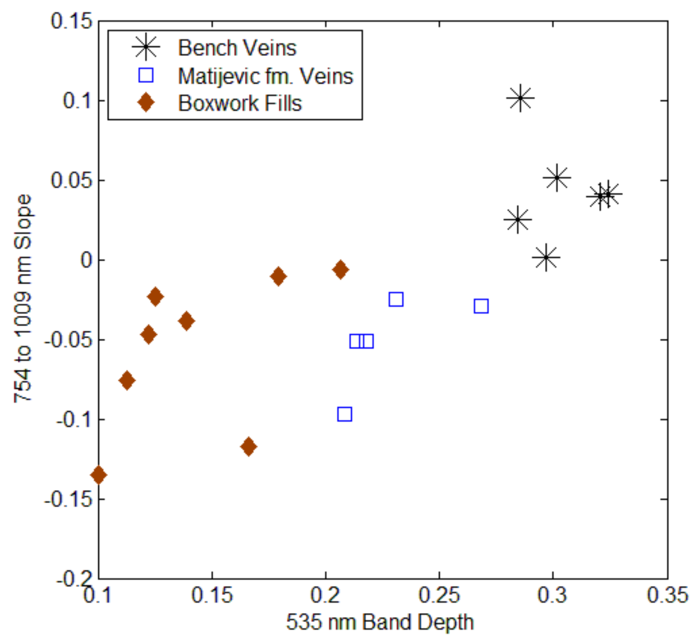

Figure 21B.

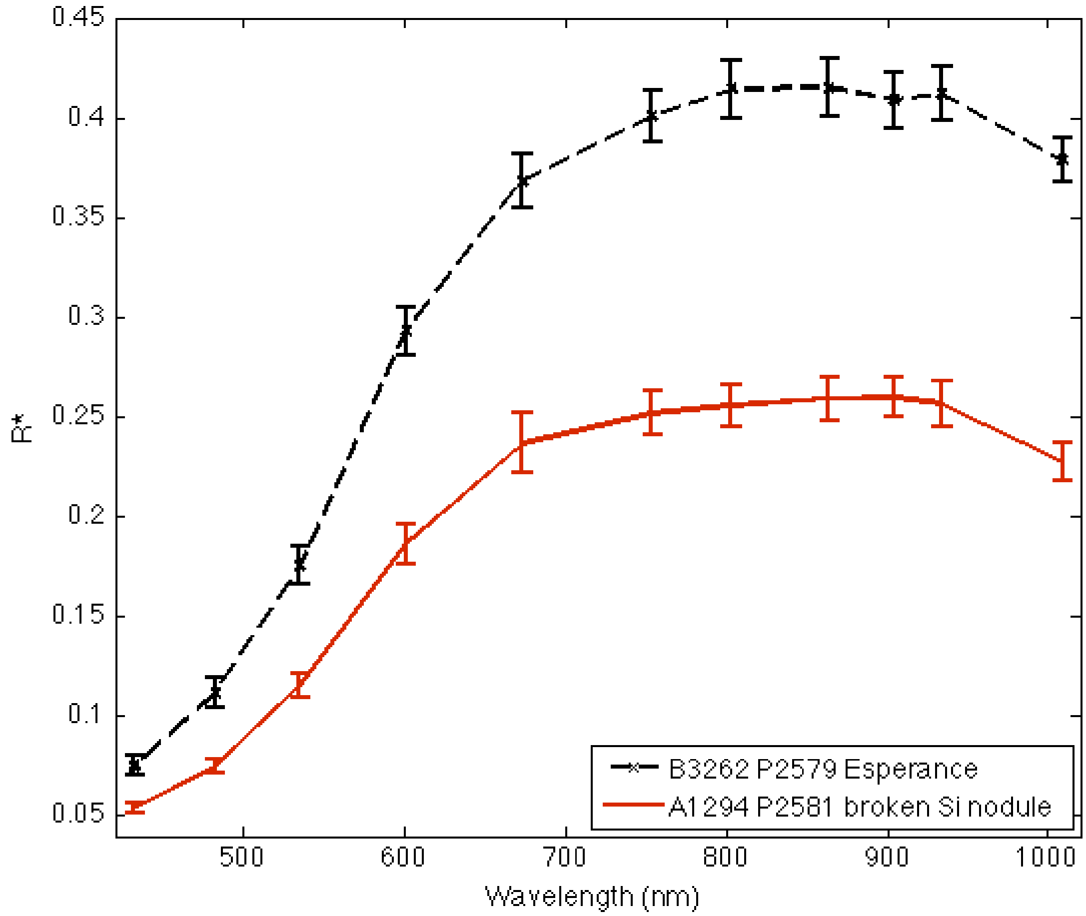

1027

1028 Figure 22.

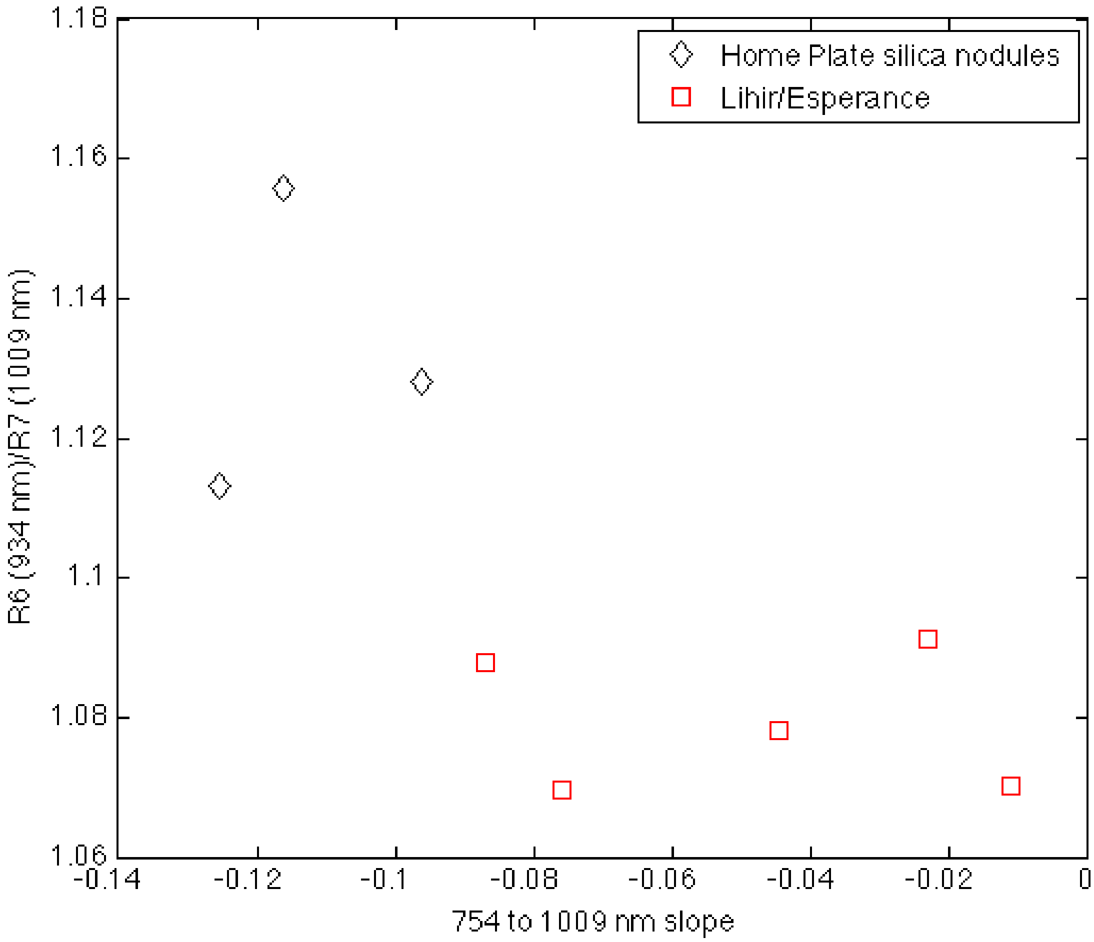
Home Plate silica nodules
Lihir/Esperance
R6 (934 nm)/R7 (1009 nm)
754 to 1009 nm slope
1.18
1.16
1.14
1.12
1.1
1.08
1.06
-0.14
-0.12
-0.1
-0.08
-0.06
-0.04
-0.02
0

Figure 23.